ADVANCED HEALTHCARE MATERIALS
www.advhealthmat.de

Microneedles for Transdermal Biosensing: Current Picture and Future Direction

*Letizia Ventrelli, Lucanos Marsilio Strambini, and Giuseppe Barillaro**

A novel trend is rapidly emerging in the use of microneedles, which are a miniaturized replica of hypodermic needles with length-scales of hundreds of micrometers, aimed at the transdermal biosensing of analytes of clinical interest, e.g., glucose, biomarkers, and others. Transdermal biosensing via microneedles offers remarkable opportunities for moving biosensing technologies and biochips from research laboratories to real-field applications, and envisages easy-to-use point-of-care microdevices with pain-free, minimally invasive, and minimal-training features that are very attractive for both developed and emerging countries. In addition to this, microneedles for transdermal biosensing offer a unique possibility for the development of biochips provided with end-effectors for their interaction with the biological system under investigation. Direct and efficient collection of the biological sample to be analyzed will then become feasible in situ at the same length-scale of the other biochip components by minimally trained personnel and in a minimally invasive fashion. This would eliminate the need for blood extraction using hypodermic needles and reduce, in turn, related problems, such as patient infections, sample contaminations, analysis artifacts, etc.
The aim here is to provide a thorough and critical analysis of state-of-the-art developments in this novel research trend, and to bridge the gap between microneedles and biosensors.

1. Introduction

Biosensing technologies will be to the first half of the 21st century what microelectronics was to the latter half of the 20th century. Integrated circuits have allowed electrical devices to shrink from room-size to pocket-size, continuously increasing in speed and nearly penetrating into aspects of everyday life. Similarly, biochips will allow many of the expensive chemical and biological analyses that are currently performed in conventional laboratories to be carried out in a hand-held, low-cost chip, with a tremendous potential impact in, though not limited to, clinical diagnostics and, in turn, public healthcare.[1–3] Today, such a vision is strongly supported by pressing requests from different levels (e.g., political, commercial, medical, etc.) for the development of novel technologies aimed at the manufacture of miniaturized chips. These would radically transform clinical diagnostics into a more efficient and less expensive practice, as clearly highlighted by the analysis of the biochip market, which is expected to reach nearly $9.6 billion by 2016, compared with a 2010 value of $3.5 billion.[1,4]

Biochips claim significant advantages over standard clinical diagnostic tools, such as lower cost and reduced power dissipation, smaller size and lower weight, smaller amount of fluid needed and shorter response time. Biochips also foresee an increase in operability by minimally trained personnel, enabling point-of-need analysis and, in turn, reducing health system costs in already developed countries. Meanwhile, in agreement with World Health Organization (WHO) guidelines, sophisticated analytical techniques would be made available in rural areas and emerging countries, where conventional laboratories are lacking.[5,6] In spite of these promises, sampling of biological fluids to be analyzed still requires the use of clinical hypodermic needles, which somehow limits biochip advantages, e.g., in terms of the reduced amount of fluid needed for analysis, reduced amount of waste, operation by minimally trained personnel, poor patient compliance due to needle pain, etc.

Microneedles, which are a miniaturized replica of clinical hypodermic needles down to the micrometer scale, offer a possibility to move beyond such limitations by providing biochips with end-effectors for minimally invasive transdermal interaction with the biological system under investigation, on the same length-scale as other biochip components. The integration of microneedles in biochips envisages a novel class of transdermal biosensors for both in situ (using the microneedles as an active component of the biosensor) and ex situ (using the microneedles to sample and fetch the biological fluid to the biosensor) pain- and risk-free measurements of analytes of clinical interest upon insertion of the needles in superficial layer of the skin. In the last decade, microneedles have been shown (in human volunteers) to increase both compliance towards skin puncture, with skin penetration perceived as (nearly) pain-free,

Dr. L. Ventrelli, Dr. L. M. Strambini, Prof. G. Barillaro
Dipartimento di Ingegneria dell'Informazione
Università di Pisa
Via G. Caruso 16, 56122 Pisa, Italy
E-mail: g.barillaro@iet.unipi.it
Prof. G. Barillaro
Istituto di Fisiologia Clinica
Consiglio Nazionale delle Ricerche
via G. Moruzzi 1, 56124 Pisa, Italy

DOI: 10.1002/adhm.201500450

and operability by non-trained personnel, with application to the skin being (mainly) risk-free.[7,8]

Although the microneedle concept dates back to the 1970s,[9] it was experimentally validated only in the mid-1990s thanks to the progress of micro- and nanotechnologies that have provided suitable tools for the fabrication of such small structures with high accuracy, high reproducibility, and low-cost methods.[8,10,11] Microneedles have so far been fabricated from various materials (e.g., silicon, metal, polymers) with different lengths (from hundreds of microns to a few of millimeters), shapes (e.g., cylindrical, conical, pyramidal), and features (e.g., solid, hollow, dissolving). Over the last decade, they have mostly been used for the effective transdermal delivery of a number of drugs and compounds (e.g., insulin, proteins, DNA, vaccines, and others), as detailed in excellent review papers.[12–14]

Very recently an increasing number of studies is being published on the use of microneedles for transdermal biosensing applications, aimed at fast, reliable, and pain-free measurements of parameters of clinical relevance (such as levels of glucose, biomarkers, and ion concentrations) both in peripheral blood and interstitial fluid (ISF).

Although a few excellent reviews have recently been published concerning the minimally invasive monitoring of glucose,[8,15] as well as the miniaturization of biochips for point-of-care applications,[1,16] their focus was not on transdermal biosensing, and small room was left for microneedles.

The aim of this study is to critically analyze state-of-the-art developments on the use of microneedles for transdermal biosensing applications, so as to bridge the gap between microneedles and biosensors. The organization within provides the reader with a clear and logical path starting from a description of the skin, which is the main organ of interest for microneedles targeting transdermal biosensing. The study proceeds with descriptions of the different typologies of microneedle-based biosensors, which are differentiated on the basis of the target analytes, and ends with a critical analysis of state-of-the-art microneedle-based biosensors, with the aim to point out future directions. In more detail, Section 2 provides the necessary details on skin microanatomy and microcirculation that are believed to be relevant to transdermal biosensing via microneedles, by taking into account skin penetration issues of such tiny needles. Section 3 reviews transdermal biosensing through microneedles with particular emphasis on minimally invasive detection of glucose and biomarkers, then clustering all other analytes sensed using microneedles in a further paragraph. Section 4 presents our own vision of transdermal biosensing via microneedles for both present applications and future research. Finally, the whole work is briefly summarized in Section 5.

Letizia Ventrelli is a post-doctoral researcher in the Information Engineering Department of the University of Pisa with the group of Prof. G. Barillaro. She received her PhD in Innovative Technologies: "Biorobotics" from the Scuola Superiore Sant'Anna of Pisa in 2013. Her main research activities are the modeling and characterization of micro/nanostructured devices and systems for biomedical and nanomedicine applications.

Lucanos M. Strambini is a Junior Researcher at the Information Engineering Department of the University of Pisa with the group of Prof. G. Barillaro. He received his PhD in Information Engineering from the University of Pisa in 2007. His main research activities concern the fabrication, characterization, and modeling of microneedles and photonic crystals for minimally invasive biosensing applications, as well as of silicon-based micro and nanostructured devices and systems for microelectronic and environmental monitoring applications.

Giuseppe Barillaro is Professor of Biomedical Electronics at the Information Engineering Department of the University of Pisa, where he has been faculty member since 2005. He received his PhD in Information Engineering from the University of Pisa in 2002. The primary research interest of Prof. Barillaro's group is to exploit micro and nanotechnologies for the development of novel materials, devices, and systems with applications in photonics, microelectronics, (bio)sensing, and medicine.

2. Skin as an Organ for Minimally Invasive Biosensing

The skin is the largest organ in the human body. Although it is generally less than 2000 μm thick, the skin accounts for about 15% of the body total weight and has a surface area of about 2 m^2. Skin is also one of the more complex organs of the human body. At least five different cell types characterize its structure and other cell types from the systemic circulation and the immune system may be resident passengers within the skin. Skin has several important functions (e.g., thermoregulation, sensory organ, endocrine tasks), the most important being to form an effective protection against external physical, chemical, and biological assaulters, as well as to control the inward

DOI: 10.1002/adhm.201500450

and outward flow of water, electrolytes and various other substances.[17]

Understanding the organization of the skin at the microscale level, inferring the spatial distribution of fluids (blood and ISF) in it, as well as knowing the mechanical properties of the different layers assembling the skin, is of chief importance for the appropriate use of microneedles for transdermal biosensing applications, both in terms of the mechanical design of the microneedles, and the compartmental site of investigation in the skin.

2.1. Microanatomy of the Skin

Mammalian skin forms the outer covering of the body and consists of two major layers.[18] The outermost layer is an epithelium called the epidermis, and the innermost layer is a connective tissue called the dermis. Skin is a dynamic organ in a constant state of change, with the cells of the outer layers being continuously shed and replaced by inner cells moving up to the surface. It also varies in thickness according to its anatomical site and the age of the individual, although its structure is consistent throughout the whole body. **Figure 1** shows a sketch of the main layers of the skin.

The epidermis comprises a multilayered epithelium, the interfollicular epidermis, and associated (adnexal) structures, i.e., hair follicles, sebaceous glands, and sweat glands. Key functions of the epidermis are the formation of a protective interface with the external environment, lubrication of the skin with lipids, and thermoregulation by hairs and sweat. The epidermis is constituted by keratinocytes (95%), melanocytes, antigen-presenting Langerhans cells, Merkel cells and stem cells (≤5%). The epidermis, whose thickness varies between 50 and 150 µm (palms and soles excluded) depending on the body site, is divided into five different layers, according to the stage of keratinocyte maturation and differentiation. The innermost layer of the epidermis, namely stratum basale, lies adjacent to the dermis and mainly consists of keratinocytes arranged in a single layer and attached to the basement membrane by hemidesmosomes. Merkel cells, which are closely associated with cutaneous nerves, are also found in the basal layer, particularly in touch-sensitive sites such as fingertips and lips. As keratinocytes divide and differentiate in the basal layer, they move through the other layers of the epidermis, namely stratum spinosum, stratum granulosum, and stratum corneum, gradually losing the abundant desmosomes and accumulating granules of keratoialin in the stratum granulosum, to lose their nucleus becoming terminal-stage keratinocytes, i.e., corneocytes, in the stratum corneum. Langerhans cells, which are immunologically active and play a significant role in immune reactions of the skin acting as antigen-presenting cells, are present in the stratum spinosum, mainly located in the middle of this layer.

In human skin, the stratum corneum is the outermost layer of the epidermis and typically consists of a stack of 18–21 layers of corneocytes, each corneocyte having a diameter of 20–40 µm. These are flat, enucleated cells packed with keratin filaments and surrounded by a thick envelope composed of insoluble loricrin and involucrin as well as covalently bound lipids. The tortuous and irregular appearance of corneocytes enables the

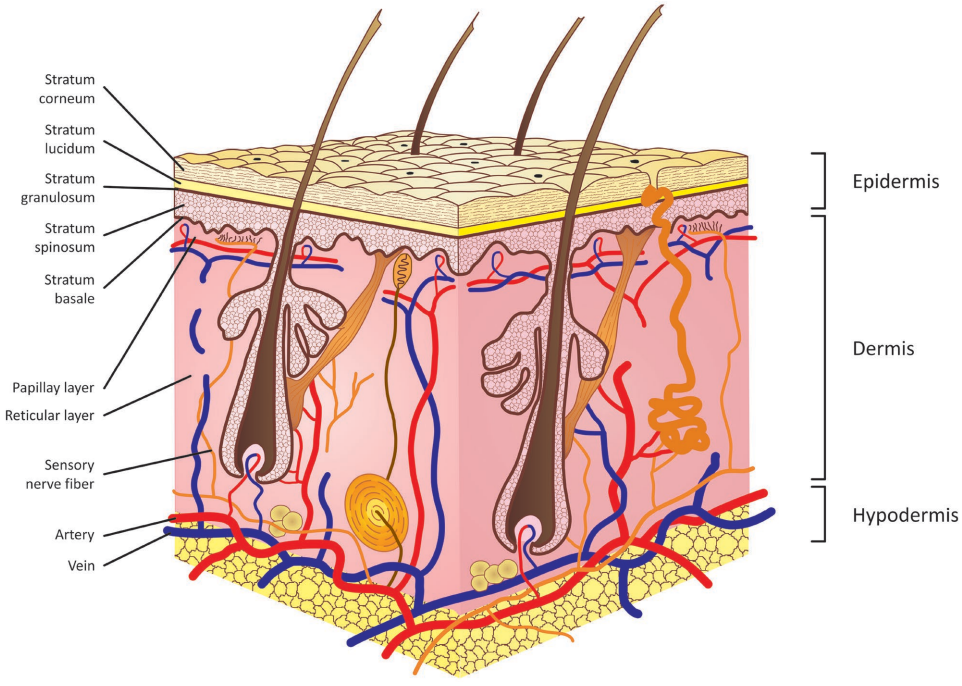

Figure 1. Sketch of the outermost layers of the human skin. Moving from the outside to the inside: the epidermis, consisting of stratum corneum (the outmost layer), stratum lucidum, stratum granulosum, stratum spinosum, and stratum basale; the dermis, consisting of papillary and reticular layers; and the superficial fascia of the hypodermis. The sketch also highlights the dermal vasculature of the skin, consisting of two intercommunicating plexuses, namely the superficial plexus and lower plexus.

overlapping of the cells, which are able to form clusters of cells grouped and overlapped at the level of lateral boundaries, in order to improve the stability of the stratum. In addition, cell-to-cell cohesion is further enhanced by the presence of corneodesmosomes, especially within the inner stratum corneum. In contrast, slow degradation of these structures in the outer stratum corneum allows the normal process of desquamation. Differences in thickness, the degree of keratin packaging, and the number of corneodesmosomes depend on the body site and on their location within the stratum corneum. Beyond the possibility to permeate minimally through hair follicles or gland excretory ducts contained in the context of the skin, all compounds must primarily cross the stratum corneum to reach the systemic circulation.[17]

The epidermis is separated from the dermis by a basement membrane, an extracellular matrix that is rich in type IV collagen and laminin.

The dermis, which lies underneath the epidermis, is about 500–2000 µm thick depending on the body site. It is composed of fibroblasts, which are the main resident cell types of the dermis, collagens and elastic fibers, bathed in a ground substance composed of gelatinous proteoglycans and glycoproteins. Histiocytes, antigen presenting cells, mast cells and infiltrating leukocytes may be also present in varying amounts. The dermis is a complex structure composed of two layers: a thin superficial papillar layer, located below (and connected with) the epidermis and rich in blood vessels and sensory nerve endings; a thick deeper reticular layer, which is formed by micrometer-long fibrous bundles whose function is to surround and support eccrine and apocrine glands, immunologically active cells, nerve endings, dermal lymph nodes, and blood capillaries. The deepest dermal layer, historically termed the hypodermis, is the thickest layer of the skin. It invaginates into the dermis, to which it is attached by collagen and elastin fibers. It is essentially composed of adipocytes grouped together in lobules separated by connective tissue. The hypodermis represents a storehouse of energy and can be up to 30 000 µm in thickness depending on the body site.

2.2. Extracellular Fluids in Skin

The epidermis is an avascular skin region. The epidermis is usually divided into stratum corneum, which is considered a physical barrier of dead cells with a "bricks and mortar" structure, and viable epidermis, which consists of the underlying epidermal layers, for which a certain enzymatic and metabolic activity has been reported. Despite recent evidence showing considerable biochemical activity within the stratum corneum,[19–21] this distinction is still used. An important difference between the stratum corneum and viable epidermis lies in the different polarity of these two layers: the former is predominately lipophilic in nature, whereas the latter is principally hydrophilic.

The dermis is the most vascularized region of the skin. The dermal vasculature is made up of two intercommunicating plexuses: the superficial plexus, located at about 300–600 µm from the skin surface at the junction of the papillary and reticular dermis, and the lower plexus, located at about 1300–1500 µm from the surface at the dermal-subcutaneous interface. The superficial plexus supplies blood to the epidermis through small capillary loops in the papillar dermis. The lower plexus is supplied by larger blood vessels from the underlying muscles and subcutaneous fat, and is directly connected to the superficial plexus through a network of arterioles and venules. The blood vessel distribution, as a function of the depth, is considerably higher in the sub-epidermal papillar dermis than in the reticular dermis,[22] with a maximum at a depth of about 100–150 µm from the surface, i.e., within the area of papillar dermis just below the basal layer.[23] Afterward, the blood vessel distribution decreases continuously and almost exponentially in the deeper layers.

The blood in the skin mostly comes from the capillaries of dermis, with a small amount of blood from arterioles and venules. Significant differences have been reported between the concentrations of various constituents in systemic and capillary blood, in healthy young adults.[24] On the one hand, the differences for total protein, bilirubin, calcium, sodium and chloride have been found to be highly important, although smaller than 5%. On the other hand, concentrations of potassium, phosphorus, urea and glucose have been found to be almost identical in capillary and systemic blood.

Blood only contributes for 5% of the skin volume fraction, whereas about 45% of the volume fraction of the human skin is constituted by ISF, with a higher amount in the dermis than in the subcutaneous tissue.[25] ISF is formed by blood transcapillary filtration and cleared by lymphatic vessels. The transcapillary exchange and formation of ISF is determined by properties of the capillary wall, hydrostatic pressure, and protein concentrations in the blood and interstitium. The interstitium, located between the capillary wall and cells, consists of a predominantly collagen fiber framework, a gel phase of glycosaminoglycans, a salt solution, and plasma proteins. ISF transports nutrients and waste products between cells and blood capillaries, signaling molecules between cells, and antigens and cytokines to local draining lymph nodes for immune regulation. Its composition and biophysical properties vary between organs and in tissue development, pathogenesis, inflammation, and remodeling as well as over normal functional cycles.[26] The composition of ISF is similar to that of plasma, although with significant differences both in terms of steady-state concentration level (concentration domain) and concentration level over time (time domain), due to factors accounting for trans-capillary flow of analytes and proteins from blood to ISF. The concentration of proteins in ISF is lower than in plasma (about one-third), and the concentrations of calcium, magnesium, sodium, and potassium are also lower, in agreement with classical physical chemistry theory.[27] Glucose levels in ISF parallel those in blood at steady-state conditions, whereas rapid changes of blood glucose levels are reflected in ISF with a variable lag time due to diffusion of glucose from capillary endothelium to ISF in the presence of a certain concentration gradient.[28,29]

2.3. Microneedle Insertion in Skin

The efficiency of microneedles in detecting analytes either resident or passenger within the skin is dependent on an effective

Adv. Healthcare Mater. 2015,
DOI: 10.1002/adhm.201500450

and reliable insertion of the needles into the skin tissue at a specific depth. To successfully achieve this goal, a particular challenge is to tailor the mechanical insertion of the needles through the skin on the basis of skin mechanical characteristics, mainly Young's modulus and breaking stress. A complicating factor is that skin breaking stress and Young's modulus have been found to significantly vary on this scale throughout the skin strata, and also with the needle radius[30,31] and strain rate.[32,33]

From a mechanical point of view, skin is a heterogeneous, anisotropic, and non-linear viscoelastic material. Furthermore, the two layers of the human skin, i.e., the epidermis and dermis, are extremely different not just in terms of thickness but also of mechanical properties, which are still under debate and subject to renewed interest thanks to the recent emergence of micro-devices for vaccine delivery into upper layers of the skin with increased immune responses. Concerning the epidermis (thickness between 50 and 150 μm), the stratum corneum (thickness about 10–20 μm) has been reported as a stiff layer with a Young's modulus between 1 and 1000 MPa, depending on the hydration level, penetration depth, and needle radius,[30,34,35] whereas the viable epidermis (thickness between 30 and 130 μm) has been reported to be significantly less stiff, with a Young's modulus between 2 and 20 MPa.[31] The dermis (thickness in the range of 500–2000 μm) has been reported to have a Young's modulus of a few tens of kPa, and hypodermis (thickness up to 30 000 μm) of a few kPa.[36] The thickness of both the epidermis and dermis is significantly dependent on body region and, for the latter, also on the alimentary diet.

An additional factor related to mechanical properties of the skin is its viscoelasticity, which has been reported to be of particular importance for microneedle penetration in skin. Viscoelasticity relies on the ability of skin to relax and lower stress upon indentation with microneedles. Quantification of the elastic properties of full-thickness skin at a micro-scale level using probes with radii from 0.5 to 20 μm has shown that skin's viscoelastic response is scale-independent, with a fast relaxation of about 40% over 1 s followed by a further 10% reduction over 10 s. Furthermore, a high scale dependency of the elastic modulus of skin was found, from about 30 MPa for the smallest 0.5 μm radius probe to about 1 MPa for the largest 20 μm radius probe.[35] Mostly due to the non-linear viscoelastic behavior of the skin, it has been found that to effectively and reliably insert microneedles (especially for densely packed arrays of microneedles) in the skin, high-velocity applicators are required, capable of inserting the needles into the skin with application rates from a few m s^{-1} up to 10 m s^{-1}.[33,37] In general, at low application (strain) rates microneedle arrays yield limited mechanical penetration due to significant skin deflection.[38,39] Conversely, increased mechanical compressive resistance at higher application (strain) rates significantly improves penetration of microneedle arrays into the skin.[32,40] As a result, spring-loaded mechanical applicators have been successfully designed and used to insert high-density (spatial period around 100–200 μm) microneedle arrays through the different layers of the skin at velocities between 1 and 10 m s^{-1} with high yields (>95%) for their full length (up to 150 μm).[33,37]

3. Transdermal Biosensing with Microneedles

3.1. Glucose Sensing

In their early stages, microneedles have mainly been used for the extraction of extracellular fluids, either blood or ISF, on which the glucose content was measured either in-line by integrated biosensors or off-line by standard commercial methods. Besides this, an increasing number of works has recently been reported on the use of microneedles for in situ monitoring of the glucose content in extracellular fluids. Microneedles for glucose monitoring have been proposed as an alternative to current blood glucose self-monitoring devices (GSMDs), mainly finger sticks performing amperometric measurements on capillary blood with poor compliance by diabetic patients (DPs) because of pain and inconvenience with repetitive blood collection (e.g., a minimum of four tests per day are necessary for patients undergoing insulin therapy).[41,42] Microneedle-based glucose biosensors have envisaged the possibility of effectively enabling a strict glycemic control in DPs by eliminating pains, thereby improving compliance and reducing the risk of diabetes complications and, in turn, deaths.[43–46]

A classification of microneedle-based glucose biosensors is given in the following based on the targeted extracellular fluid, either blood or ISF, regardless of whether the microneedles were hollow or solid.

3.1.1. Blood-Targeting Microneedles

In view of the application of microneedles for blood analysis, in 2001 Kobayashi et al.[47] reported the development of a microsystem integrating a single out-of-plane hollow platinum (Pt) microneedle making use of a sampling mechanism employing a phase-transition gel together with a glucose oxidase (GOx) enzyme-based biosensor for the measurement of the glucose level (**Figure 2**). The microsystem (overall dimension 15.1 mm × 18.1 mm) was obtained by bonding together a silicon substrate integrating the sampling mechanism and a glass substrate integrating the on-chip glucose biosensor, with the needle protruding from the chip. A microcontainer for the phase-transition gel was fabricated on the silicon substrate through anisotropic etching techniques. The microcontainer was connected to the needle through an inlet flow channel formed with an 80-μm-thick SU-8 layer with rectangular section and a width linearly variable from 1 mm at the needle side up to several millimeters at the microcontainer side. Two outlet flow channels with rectangular sections and widths of 1 mm connecting the microcontainer to the side edge of the chip were formed in the SU-8 layer perpendicularly to the inlet channel, and were used to remove the solution overflowing from the gel. The glucose biosensor was fabricated on the glass substrate and was able to detect glucose through the measurement of hydrogen peroxide produced by the enzymatic reaction catalyzed by GOx. The working electrode (Pt), the auxiliary electrode (Pt) and the reference electrode (Ag/AgCl) were patterned by standard photolithography directly on the glass substrate. GOx was immobilized on the working electrode afterwards with 10% bovine serum albumin (BSA) and 10% glutaraldehyde. In

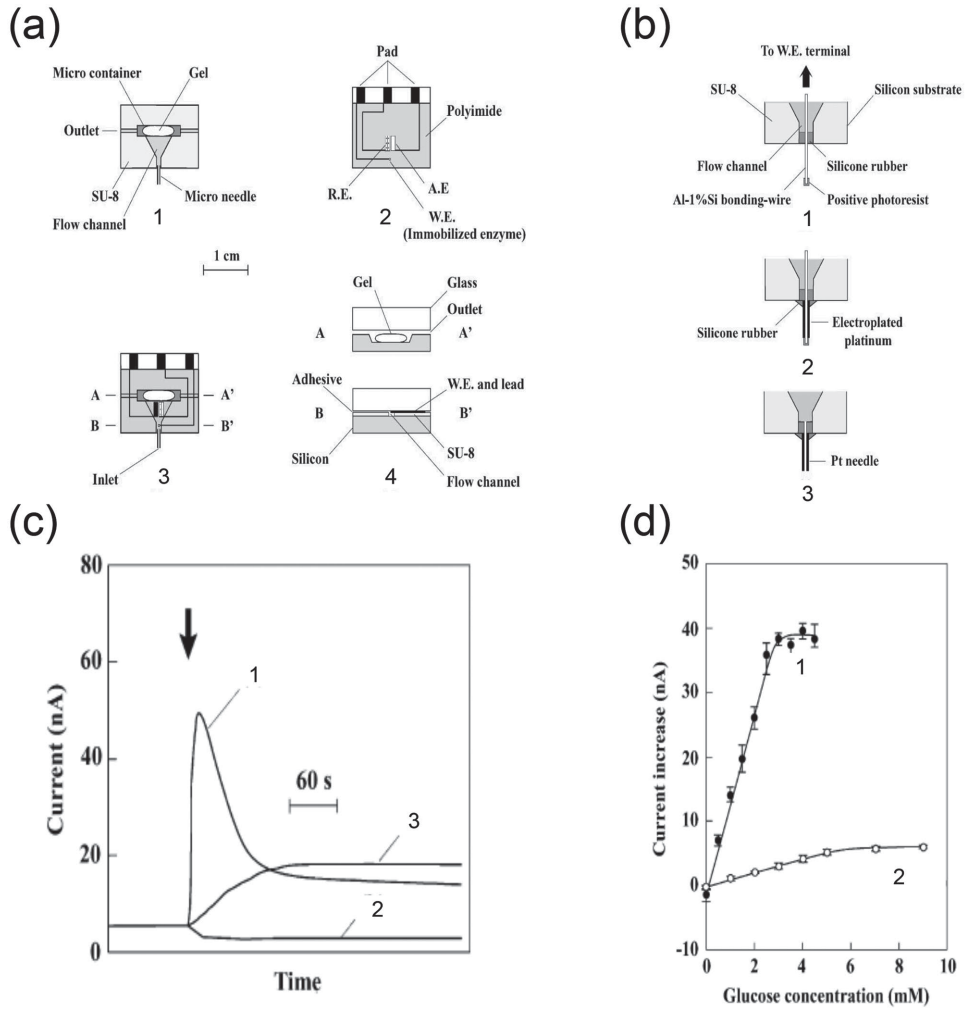

Figure 2. A mosquito-inspired microneedle-based micro analysis system for glucose monitoring. a) Structure of the microsystem in 1–3) top-view and 4) cross-section). b) Main fabrication steps of the out-of-plane hollow Pt microneedle. c) In vitro response curves of the microsystem to sampled glucose solution 1) without the microneedle, 2) without the gel and the microneedle, and 3) with the microneedle, with temperature decreasing stepwise from 40 to 30 °C. d) In vitro calibration curves of the micro analysis system at 30 °C 1) with and 2) without microneedle. Reproduced with permission.[47] Copyright 2001, Elsevier.

order to sample the solution of interest, a sampling mechanism that exploited a phase-transition polymer gel (i.e., poly(*N*-isopropylacrylamide)) undergoing volume changes in pure water induced by temperature variations was implemented by selective formation of the polymer in the microcontainer.[48] Figure 2a shows a schematic representation of the structure of the whole microsystem. Eventually, the hollow Pt microneedle with an inner diameter of 50 µm and a length of 1 mm was fabricated through Pt electrodeposition on an Al-1% Si bonding wire fixed to the inlet flow channel, which was subsequently dissolved in NaOH solution. Figure 2b presents the main fabrication steps of the Pt microneedle.

The different components of the microsystem, i.e., the sampling mechanism and glucose biosensor, were firstly independently and successfully characterized in vitro without the presence of the microneedle, using glucose solution, upon a step-wise temperature variation of the system from 40 to 30 °C. Eventually, the whole microsystem characterization was also carried out to assess the response of the on-chip glucose biosensor to glucose solution sampled through the microneedle. Either the inlet flow channel or the needle of the microsystem was filled with a buffer solution (pH = 7.4) containing 0.1 M potassium chloride (KCl) at 30 °C (control solution), which caused the gel to swell and completely fill the microcontainer. The microsystem was then put on a hotplate at 40 °C thus causing the gel to shrink and the solution to overflow out of the gel through the outlet flow channels. After the output current of the glucose biosensor was stable over time (reference value), either the inlet of the flow channel or the microneedle at the end of the system was immersed in a glucose solution at 30 °C. Following the immersion, the glucose solution was immediately sucked from the inlet of the flow channel or through the microneedle up to the biosensor (Figure 2c). By analyzing the dependence of the biosensor current on glucose concentration at 30 °C, with respect to the reference value in 0.1 M KCl at 40 °C, a linear calibration curve was obtained for

Adv. Healthcare Mater. **2015**,
DOI: 10.1002/adhm.201500450

glucose values below 2.5 mM ($R^2 = 0.991$) and 5 mM ($R^2 = 0.994$) for the microsystems without and with the microneedle, respectively (Figure 2d). In spite of the extended linear range of the latter, the microsystem with the microneedle showed a smaller sensitivity and longer response time with respect to the former case without the microneedle.

One year later, the same group[49] proposed an improved version of the same microneedle-based system, referred to as an "intelligent mosquito", that addressed some chief issues of the former version, such as the operation temperature, which was outside the normal range of body temperature, and the pumping mechanism, which was one-directional and did not allow the glucose solution to be pumped outside the microsystem. The volume-phase transition of the poly(*N*-isopropylacrylamide) gel was used to construct a reversible sampling mechanism by exploiting the elastic force of a silicone rubber layer that allowed repeated pumping of an external glucose solution in and out of the flow channel through the microneedle at operating temperatures of 37 and 30 °C, respectively. The functionality of the whole microsystem was successfully demonstrated in vitro by repeatedly sampling glucose solutions with different concentrations in the range 0–12 mM (a phosphate buffer solution with no glucose was used as control) through the microneedle and by monitoring the biosensor current in both time and amplitude domains. A linear relationship was observed between the amplitude of the biosensor current and glucose concentration up to 8 mM, thus also improving the linear range with respect to the former version of the microsystem.

The "intelligent mosquito" concept was further developed to fabricate a disposable microsystem for on-line continuous sampling and monitoring of glucose in peripheral blood.[50] The microsystem was based on the same main components of the earlier system,[47,49] i.e., a phase-transition gel sampling mechanism, a GOx enzyme-based glucose biosensor, and a Pt microneedle, with several novelties concerning the sampling mechanism so as to have a continuous and constant sampling of the solution through the microneedle. The microsystem (overall dimensions of 15 mm × 15 mm × 12 mm) consisted of a sensing module and a sampling module. The sensing module consisted of an on-chip glucose biosensor and a flow channel connecting the needle to the biosensor. The glucose biosensor was a thin-film three-electrode system with a Pt working electrode, an Ag/AgCl reference electrode, and a Pt auxiliary electrode. The sensitive area of the on-chip glucose sensor entailed three layers, namely a bottom Nafion layer to minimize the influence of interfering compounds, an intermediate enzyme-immobilized layer containing GOx, and a top diffusion-limiting membrane of poly(2-hydroxyethylmethacrylate) (polyHEMA). A stainless steel hollow microneedle (inner diameter of 50 µm, outer diameter of 130 µm, and length of 1 mm) was attached to a through-hole created at the end of the flow channel of the sensing module. The sampling module consisted of a reservoir for water or buffer solution, a microcontainer for the gel, a silicone rubber diaphragm, and a reservoir for the sampled solution. A phase-transition gel, namely poly(*N*-isopropylacrylamide) copolymerized with acrylic acid (AA), which contains ionized moieties in its backbone and features a volume change in aqueous solution upon temperature change, was used to implement a reversible micropump capable of withdrawing an external solution through the needle.[51,52] Three different options were investigated to induce a substantial volume change of the copolymerized gel at a low rate, which is required for continuous sampling applications, namely: temperature variation between 20 and 37 °C (no solvent was filled in the reservoir); both temperature variation and pH changes (10 mM Tris-hydrochloric acid (HCl) buffer solution at pH 9.0 was used as the solvent for the gel and 100 mM citrate-NaOH buffer solution at pH 3.0 was subsequently filled in the reservoir); enzymatic reaction of GOx (5 mM KH_2PO_4-NaOH buffer solution at pH 7.0 was used for the solvent of the gel and the same buffer solution containing glucose was added to start sampling). The volume change of gel containing GOx allowed the sampling rate to more effectively slow down, with respect to the other two modes of operation, being the sampling rate of the enzyme-loaded gel dependent on several factors including buffering capacity, enzyme activity, glucose concentration, and diffusion, thus providing greater freedom to control the volume change of the gel. The sampling rate in the linear region was 73 and 24 µL h^{-1} for temperature change alone, and for combined temperature and pH changes, respectively. For the enzyme-loaded gel, a sampling rate of 4 µL h^{-1} was able to withdraw the external solution continuously for nearly 10 h. The sampling mechanism was then integrated within the microsystem and the current of the on-chip glucose biosensor was recorded over time by continuously withdrawing an external solution with randomly changing glucose concentrations (namely 0, 5, 10, 15, 20 mM) into the flow channel through the microneedle. The calibration curve obtained by plotting the current amplitude versus glucose concentration was linear in the examined concentration range.

A microneedle-based blood sampling system for glucose monitoring was later reported by Tsuchiya et al.[53,54] The mechanical design of the system was inspired by the female mosquito's blood sampling mechanism, which can extract human blood through its labium. The blood sampling device consisted of: 1) a biocompatible and painless hollow titanium (Ti) microneedle with dimensions comparable to those of the mosquito's labium (length of about 1 mm, external diameter of 60 µm and internal diameter of 25 µm); 2) an indentation system making use of a shape memory alloy (SMA) actuator to force the microneedle into the skin; 3) an electrical micro pumping system to extract blood using a bimorph type piezoelectric microactuator; and 4) a GOx enzyme-based MOSFET biosensor to detect the amount of glucose in the extracted blood. The microneedle was fabricated by radio-frequency (RF) magnetron sputtering of a Ti coating (and subsequent thermal annealing) on a copper wire, which was eventually removed. An in vitro characterization of the blood extraction capability of the system was carried out using a stainless microneedle with 100 µm inner diameter both in water and whole human blood under 20 V biasing at 25 Hz. Extraction rates of about 10 µL min^{-1} (1.67×10^{-10} m^3 s^{-1}) and 2 µL min^{-1} (0.33×10^{-10} m^3 s^{-1}) for water and whole blood were obtained, respectively, which were comparable to the extraction rate of whole blood by the female mosquito (i.e., 0.15×10^{-10} m^3 s^{-1}). A preliminary demonstration of in vitro glucose detection with the system was given for a 0.5 mM glucose solution after an extraction time of 30 s. The output voltage of the MOSFET glucose biosensor was monitored over time and showed a voltage

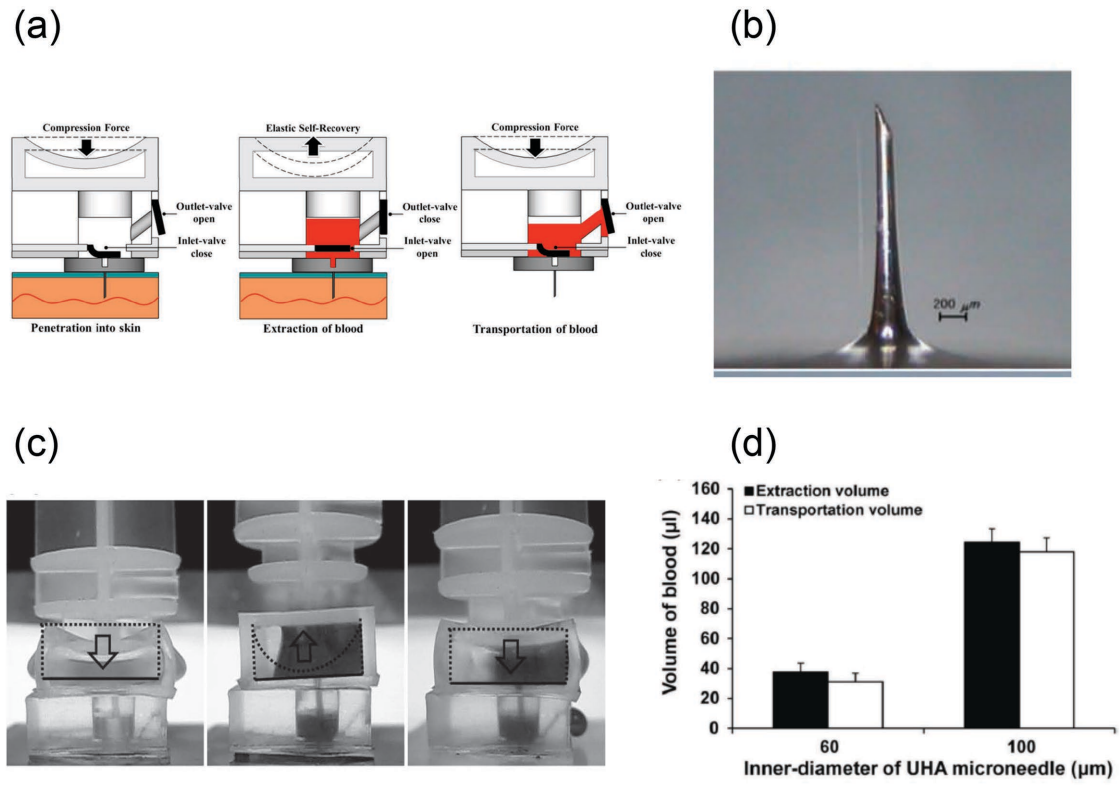

Figure 3. A minimally invasive blood-extraction system with an UHA microneedle. a) Schematic of the elastic self-recovery actuator module for blood extraction and transportation. b) Image of the UHA microneedle (60 μm inner diameter, 15° bevel angle). c) In vitro experimental extraction and transportation tests of DW. d) In vivo extraction and transportation volumes of blood from a rabbit using UHA microneedles with inner diameters of 60 μm and 100 μm. Reproduced with permission.[56] Copyright 2012, John Wiley and Sons.

peak at 30 s, then started decreasing to reach a steady-state value after 120 s. However, no calibration of the system against glucose concentration was provided.

An electronic mosquito's blood sampling microsystem for glucose monitoring was also proposed by Gattiker et al.,[55] although no characterization of the proposed system was given.

The approach of using hollow microneedles for sampling blood to perform glucose detection has somehow been overlooked for a few years due to the difficulties in achieving good reliability and accuracy. Recently, Li et al.[56] proposed a novel minimally invasive blood-extraction system by assembling an ultrahigh aspect ratio (UHA) hollow nickel microneedle in a polydimethylsiloxane (PDMS) elastic self-recovery actuator (**Figure 3**). In vivo extraction and transport of blood from a rabbit without requiring an external power source were successfully demonstrated. The system consisted of three parts: 1) a highly elastic self-recovery PDMS switch used to produce negative pressure for blood extraction; 2) a PDMS chamber with two passive valves (inlet and outlet) that controlled the extraction of blood samples into the chamber and transportation of blood into another analysis system by a hand-pump approach; and 3) a UHA hollow nickel microneedle with length of 2 mm, inner diameter of either 60 or 100 μm, outer diameter of 100 μm, and bevel angle of 15°. The whole system is sketched in Figure 3a. The hollow nickel microneedle was fabricated by preparing a high aspect ratio SU-8 photoresist mold by a drawing lithography technique, thus overcoming the length limitations of traditional microneedle fabrication technology. The mold was subsequently covered in nickel via an electroplating technique and eventually removed to obtain the hollow metallic needle[57,58] (Figure 3b). The system was tested both in vitro and on a live rabbit by pressing the PDMS switch with a finger to deploy the microneedle into an ear artery. The removal of the compressive force caused a negative pressure inside the PDMS chamber and, in turn, inside the needle, that opened the inlet valve and closed the outlet valve thus allowing blood extraction from skin and filling the chamber with the extracted blood. After collection, blood could be expelled from the PDMS chamber through the outlet valve by pressing the PDMS switch again (Figure 3c). The 60 μm needle extracted 37.7 ± 3.4 μL of blood at a rate of 3.1 ± 0.2 μL s^{-1}, whereas the 100 μm needle extracted 124.5 ± 5.1 μL at a rate of 8.3 ± 0.6 μL s^{-1}, the latter achieving a 3-fold increase in extracted blood volumes (Figure 3d). Although the blood-extraction system was not connected to an analysis device, blood extracted with the 60 μm needle (37.7 ± 3.4 μL) was successfully transported (31.3 ± 3.3 μL) through the outlet valve by re-pressing the switch, yielding a sufficient volume for further microsystem analysis.

The same group thereafter investigated the effects of different geometrical parameters, namely inner diameter, tip diameter, and bevel angle, of minimally invasive hollow metallic microneedles for blood-extraction.[59] The microneedles were fabricated by drawing lithography and subsequent

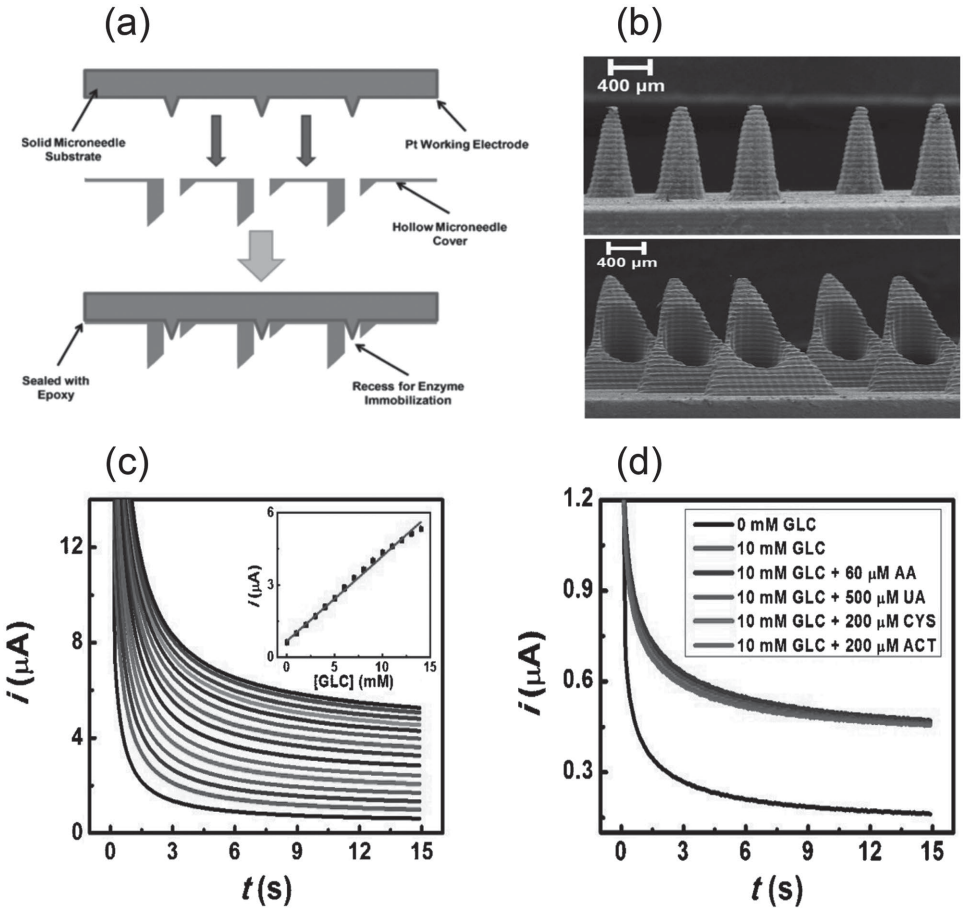

Figure 4. A bicomponent microneedle array glucose biosensor. a) Bicomponent microneedle fabrication through integration of Pt-coated solid and hollow polymer microneedles (sketch not to scale). b) SEM images of solid (top) and hollow (bottom) polymer microneedle arrays. c) In vitro sensitivity of the microneedle-based glucose biosensor for increasing glucose concentrations (0–14 mM). d) In vitro selectivity of the microneedle-based glucose biosensor in the presence of electroactive physiological interferents (AA, UA, CYS, and ACT). Reproduced with permission.[62] Copyright 2011, John Wiley and Sons.

nickel electroplating in combination with laser-cutting techniques. In vitro liquid extraction was performed using distilled water (DW), blood-mimicking fluid (BMF), which mimicked the plasma of healthy human blood with a viscosity of 4.31 ± 0.03 cP,[60] and whole human blood treated with 8% (v/v) of the anticoagulant solution CPDA-1. The effect of the inner diameter and bevel angle of the hollow microneedles on liquid extraction was analyzed using microneedles with inner diameters of 40, 60, 80, and 100 µm and bevel angles of 15, 45 and 90°. The wall thickness and length of each microneedle was fixed at 30 µm and 1800 µm, respectively. Experimental results highlighted that a microneedle with a height of 1800 µm, an inner diameter of 60 µm, an outer diameter of 120 µm, and a bevel angle of 15° was optimum in terms of both efficient blood extraction and minimally invasive operation. Microneedles featuring this geometry were strong enough to penetrate the skin without breaking and were successfully integrated into an elastic self-recovery actuator to extract mouse blood. In vivo blood extraction with such an optimized microneedle was investigated in a mouse model using an elastic self-recovery actuator to provide adequate negative pressure by controlling the actuator volume. A 20 µL volume blood sample was extracted into the chamber of the system at an extraction rate of 0.8 µL s^{-1} from the tail artery of the mouse by means of the same procedure for blood extraction described by Li et al.[56] Although the extracted volume was sufficient for micro-analysis systems,[61] both hemolysis of blood following extraction and bio-compatibility issues of nickel could be a hurdle for biomedical applications of such microneedles, which needs to be properly addressed for clinical applications.

One of the first works for in situ monitoring of glucose in blood using microneedles was given by Windmiller et al. in 2011,[62] which reported the fabrication and in vitro testing of an integrated electrochemical biosensor for glucose monitoring making use of both solid and hollow (i.e., bicomponent architecture) microneedles (**Figure 4**). The biosensor relied on an array of Pt-coated solid microneedles, which acted as the working electrode. This was arranged into an array of hollow microneedles, which was used as a cover and yielded an array of multiple microcavities (Figure 4a). Such microcavities surrounded each solid needle, thus facilitating the electropolymeric entrapment of the recognition enzyme within each microrecess. Solid and hollow microneedles were fabricated according to a standard UV rapid prototyping technique using E-shell 200 acrylate-based polymer as the constituent material. The solid needles

were cone-shaped (base diameter of 390 ± 14 μm and height of 818 ± 35 μm), whereas the hollow needles were pyramid-shaped with a triangular base (edge length of 1174 ± 13 μm, height of 1366 ± 15 μm and bore diameter of 342 ± 5 μm). Scanning electron microscopy (SEM) images of both solid and hollow polymer microneedles are shown in Figure 4b. Both solid and hollow needles were prepared in 3 × 3 square arrays with spatial period of 2 mm. High uniformity of the needle morphological and geometrical features was achieved, as was determined from the SEM analysis. After fabrication, the surface of the solid microneedles was coated with a thin film (≈12 nm) of Pt using pulsed laser deposition (PLD),[63] so as to provide the device with a working electrode. The solid needles were eventually arranged within the borehole of the hollow needles under an optical microscope, thus obtaining a bicomponent microneedle array with solid needles protruding from hollow ones, surrounded by recess microcavities. These latter allowed for the effective entrapment of GOx enzyme into a poly(*o*-phenylenediamine) (PPD) thin film deposited by subsequent electrochemical polymerization. The PPD-based enzyme entrapment methodology ensured high selectivity and good stability through the rejection of coexisting electroactive interferences generally present within body fluids.[64] The bicomponent microneedle array biosensor was calibrated by chronoamperometric detection of glucose with concentrations in the range 0–14 mM, in phosphate-buffered saline (PBS) solution (Figure 4c). A well-defined response, characterized by a linear calibration curve (R^2 = 0.996) with a high sensitivity (0.353 μA mM^{-1}) and a low standard deviation (RSD = 6.44%, n = 3) along with a limit-of-detection (LOD) of 0.1 mM (signal-to-noise ratio, S/N = 3), was obtained over the entire range of tested concentrations. High selectivity was observed in the presence of potential electroactive interferents, such as ascorbic acid (AA), uric acid (UA), cysteine (CYS), and acetaminophen (ACT) at physiological levels, which resulted in negligible deviations (in the range of 0.88–2.21%) from the current response at 10 mM glucose (Figure 4d). Finally, a time-stability analysis of the GOx-functionalized microneedle array biosensor was carried out in a buffer solution containing 10 mM glucose over an 8-hour time period. A highly stable current response was yielded, retaining 97% of the original signal level over the whole time period.

A similar microneedle platform was reported by Invernale et al.,[65] which developed a microneedle-based biosensor for in situ amperometric detection of glucose. Stainless steel (316L grade) linear arrays of solid microneedles (length of 680 μm and width of 250 μm) were purchased and subsequently covered with Pt (thickness of 450 nm, on top of a 50-nm-thick Ti base) by sputter coating. A conducting polymer, namely poly(3,4-ethylenedioxythiophene) (PEDOT), was used as an electrical mediator for glucose sensing, as well as an immobilization agent for the glucose-specific enzyme GOx. Conducting polymers were chosen due to their unique advantages toward immobilization and signal transduction without loss of signal over time, unlike small-molecule mediators such as quinones.[66] Moreover, swelling of conducting polymers in water was sufficient to allow the diffusion of glucose to the enzyme for signal transduction but not the escape of large enzymes from the polymer film. This allowed the immobilized enzyme to be kept stable so as to not denature or contort, thereby losing its function. PEDOT was electrochemically polymerized on both bare stainless steel and Pt-coated microneedles using a polymerization solution containing GOx, which resulted in the immobilization of thin GOx films within an electrically conducting polymer matrix. The microneedle-based biosensors were then tested in vitro using a 2 mM solution of glucose in PBS to make sequential glucose additions. Chronoamperometry was employed to monitor current changes over time, corresponding to each addition of glucose until a steady-state stable value was reached, the latter used to correlate current values to glucose concentration values. Pt-coated microneedles showed improved performance with respect to bare stainless steel microneedles, with high linearity between 36 and 432 mg dL^{-1} of glucose, almost covering the physiological range of 0–432 mg dL^{-1} of glucose for diabetic patients, and good S/N ratio (10.7). Investigation of the effect of various interferents in human blood highlighted that glucose exhibited a far higher signal than any other analyte found in blood. Long-term stability of the microneedle-based glucose biosensors was also evaluated by storing the microneedles for 1, 3, and 7 days either in PBS (wet storage) or in an empty vial (dry storage) at room temperature prior to performing glucose detection. The performance of the Pt-coated microneedle sensors was not significantly altered by either wet or dry storage conditions, still maintaining high linearity and S/N ratios, contrary to bare steel microneedle sensors that demonstrated relatively poor performance. However, Pt-coated steel microneedles stored in dry conditions had shortened ranges (252 mg dL^{-1}) with respect to those stored in wet conditions (396 mg dL^{-1}), though they showed same linearity. The biocompatibility of the proposed microneedle biosensors was eventually assessed by means of a cytotoxicity assay after 1, 3, and 7 days of storage in PBS that showed no statistically significant changes in cell viability, thus concluding that no toxic effects from the PEDOT-coated microneedles were produced.

An original microneedle-based three-electrode integrated enzyme-free sensor and its in vitro characterization for glucose detection was reported by Yoon et al.[67] (**Figure 5**). A 15 × 15 array of sharp silicon microneedles (height of 380 μm and tip dimension smaller than 1 μm) was produced through anisotropic dry etching of patterned silicon chips, which was used to fabricate an array of silicon pillars. This was followed by isotropic face-up/face-down wet etching of the silicon micropillars, which was used to obtain an array of sharp silicon microneedles (Figure 5b). A 500-nm-thick silicon dioxide (SiO_2) layer was then conformally deposited on the needle surface via plasma-enhanced chemical vapor deposition (PECVD), onto which a 5-nm-thick iron catalyst was deposited via electron beam evaporation in a selected area of the array (through a shadow mask) to create the working electrode (WE) and counter electrode (CE). A vertically aligned forest of 135-μm-tall multiwalled carbon nanotubes (MWCNTs) was directly grown on the iron-coated silicon microneedle array so as to increase the electroactive surface area of the electrodes (Figure 5c). Finally, Pt nanoparticles (diameters in the range of 50–100 nm) were electrodeposited on the electrode surface so as to enhance non-enzymatic electrochemical glucose sensing, as demonstrated by Kim et al.[68] After formation of the WE and CE, a 100-nm-thick Ti layer and a subsequent 300-nm-thick silver layer were selectively deposited using a second shadow mask. The silver layer was subsequently

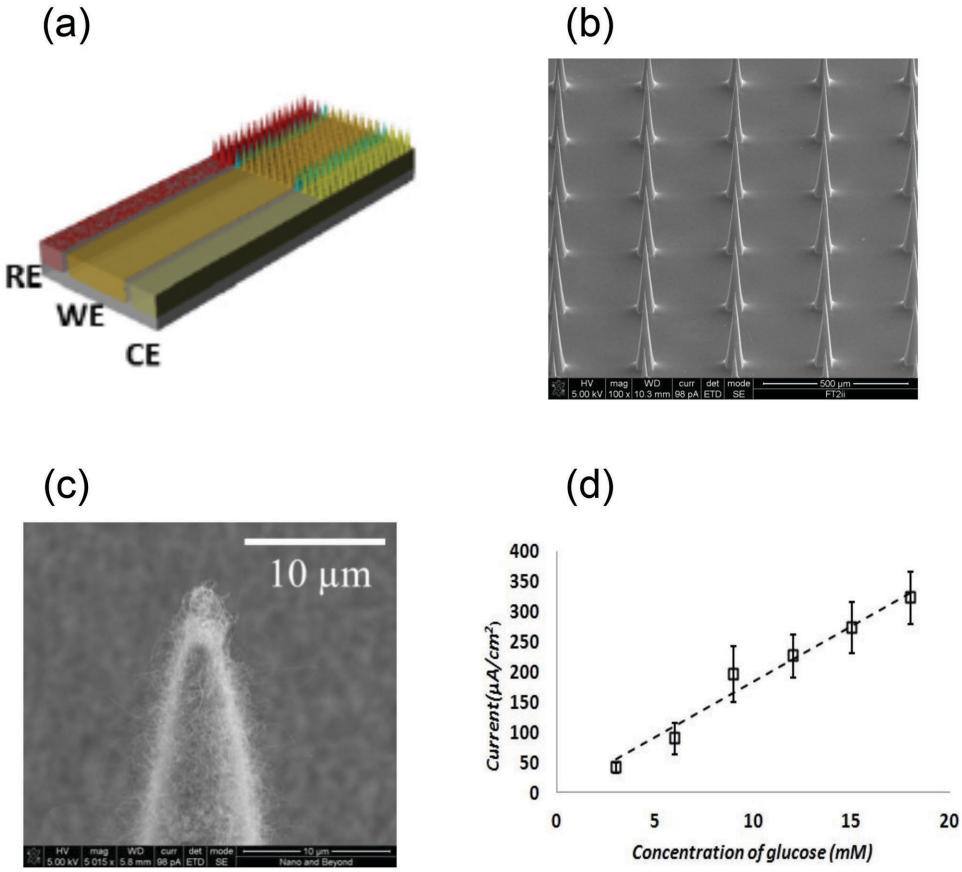

Figure 5. A three-electrode microneedle/CNT non-enzymatic glucose sensor. a) Sketch of the three-electrode microneedle sensor. b) SEM image of the bare silicon microneedle array obtained through dry/wet etch fabrication. c) SEM image of the tip of a single needle of the array coated with MWCNTs. d) In vitro calibration curve of the three-electrode microneedle/CNT glucose sensor for increasing glucose concentrations (3–20 mM). Reproduced under license CC BY 3.0.[67]

chlorinated uniformly in 1 M KCl/HCl buffer solution in order to form an Ag/AgCl reference electrode (RE) directly on the sensor. The microneedle-based three-electrode sensor was tested in vitro using different glucose concentrations in the range of 3–20 mM in 0.01 M PBS solution (Figure 5d). The chronoamperometric response of the non-enzymatic microneedle glucose sensor was investigated at a fixed potential (+0.4 V vs Ag/AgCl RE) by adding a known amount of analyte (3 mM) at regular intervals. The sensor showed a nearly linear increase of the current density as a function of the glucose concentration over the whole tested range, with a sensitivity of 17.73 ± 3 µA mM^{-1} cm^{-2}, which was higher than other non-enzymatic sensors reported in the literature thanks to the increased surface area of the Pt-decorated MWCNT forest.

3.1.2. ISF-Targeting Microneedles

As we are aware, the first use of silicon hollow microneedles for in vivo ISF sampling aimed at glucose content monitoring was reported by Zimmerman et al.[69] in 2003. The group proposed a minimally invasive continuous glucose monitoring microsystem consisting of a hollow out-of-plane microneedle array used to sample ISF from the epidermis and of an integrated enzyme-based flow-through electrochemical biosensor for the in-line monitoring of glucose content. An array of eight "volcano-like" out-of-plane hollow silicon microneedles (length of 200 µm, internal diameter of 40 µm) was fabricated by means of a technological process that combined both anisotropic and isotropic etching steps.[70] The needles were used to penetrate the outermost layers of the skin (on a finger) and sample ISF from the epidermis. Capillary and evaporation forces were exploited to enable ISF flow through the microneedles and past the integrated two-electrode enzyme-based glucose biosensor; the latter was placed in a shallow flow channel grooved into the Pyrex underneath the needles. An in-device enzyme immobilization on the sensor electrodes was carried out through the use of auxiliary flow channels. A preliminary experimental calibration of the glucose biosensor (not connected to the needles) at different glucose concentrations between 0 and 600 mg dL^{-1} highlighted a linear response in the range of 0–160 mg dL^{-1}, with an optimal flow-rate of 25 µL min^{-1}. As to the whole microsystem, a significant variation of the biosensor current was measured after the needles were inserted into the skin, thus suggesting the successful sampling of ISF through the microneedles. However, the current signal was not stable over time and started to decrease as soon as a maximum value was reached, thus demonstrating that capillary and evaporation forces alone were not sufficient to

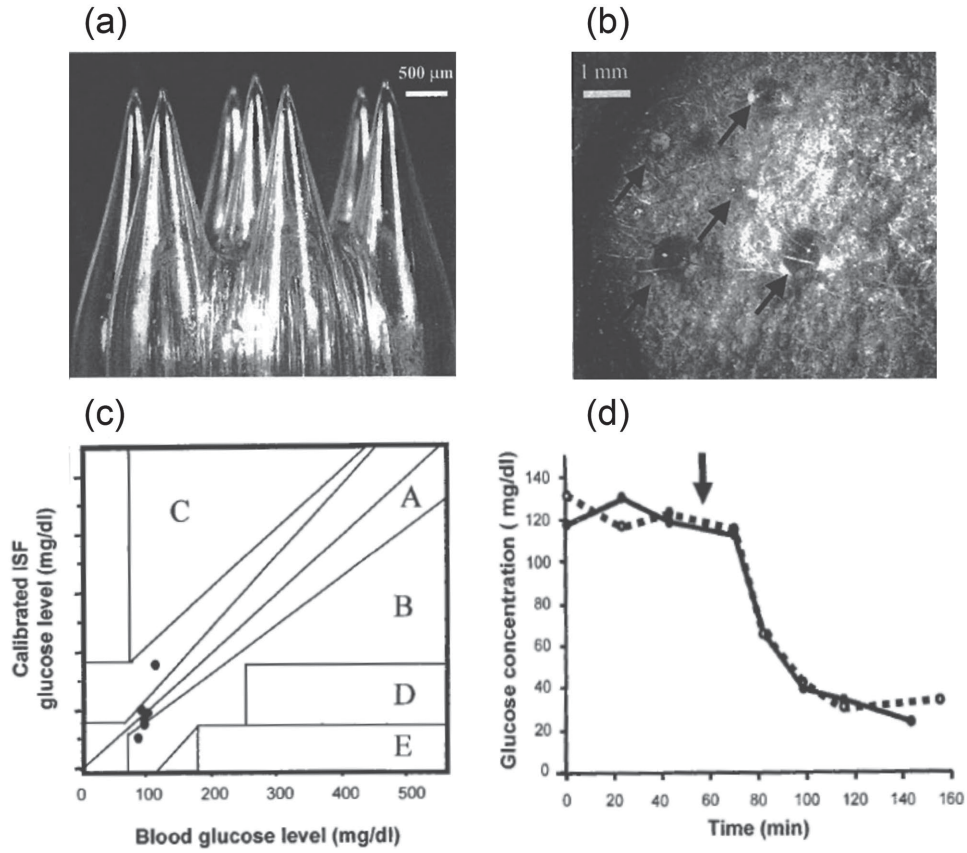

Figure 6. Glass solid microneedles for ex situ ISF-based glucose monitoring. a) Image of a multi-needle array obtained by mechanical assembling of seven single-needles. b) A bright-field micrograph of ISF droplets on hairless rat skin after piercing with microneedles and applying suction. c) Comparison between ISF and blood glucose levels in human subjects using Clarke Error Grid analysis. d) In vivo kinetic study of glucose concentration over time measured in ISF (dashed line) and blood (solid line). Reproduced with permission.[72] Copyright 2005, Mary Ann Liebert, Inc.

sustain a constant flow of ISF through the system and, in turn, a significant amount of diffused glucose over time through the biosensor. Probably due to the poor biosensor current stability over time, no calibration of the whole microsystem was reported.

In 2004, Mukerjee et al. reported the fabrication and preliminary tests of a microsystem making use of hollow silicon microneedles integrated with fluidic microchannels for ISF extraction from skin.[71] The microsystem consisted of a silicon/glass chip with dimensions of 2 cm × 1 cm × 0.1 cm. The silicon chip integrated an array of hollow microneedles intended for ISF extraction on the front-side, and a reservoir for ISF collection and storage, connected to the needles through a net of fluidic microchannels, on the back-side. The microneedles were fabricated by means of a process combining deep reactive ion etching (DRIE), diamond blade circular sawing, and isotropic etching. Needles with different shapes were produced — "volcano-like", "micro-hypodermic", and "snake-fang" — although only the "snake-fang" microneedles (20 × 20 array of needles featuring a shank height of 250–350 μm and center-to-center spacing of 300 μm) were used to demonstrate ISF extraction from skin. Solid (i.e., without bore hole) microneedles were firstly used for puncture tests by pressing the array into the human skin (first knuckle of the thumb) and imaging the puncture wounds at increasing depths with a confocal microscope. The resulting silicon microneedles were both sharp and stiff enough to pierce the stratum corneum without breaking and to allow penetration of the epidermal layers down to 160 μm. The amount of pressure needed to pierce the skin was measured to be 1.5 ± 0.25 N. To successfully demonstrate extraction of ISF from skin, the "snake-fang" microneedle array was pressed onto the author's earlobe and the chip was held in place with a spring clip for 15–20 min. A clear fluid with no visible cellular matter was visible in the back-side channels of the micro-device after extraction. In order to validate that the extracted fluid was ISF, and not some other fluid (e.g., sweat), an in situ measurement of the glucose content was carried out placing a small amount of commercial blood glucose test strip into the reservoir through a hole drilled in the glass slab. The colorimetric variation (from clear to deep blue) revealed a glucose concentration of about 80–120 mg dL^{-1} in the extracted fluid, as well as in the author's blood used as control. Conversely to what was observed by Zimmerman et al., even though an initial 20–30 min latent time was needed to generate enough ISF to fill the bore-hole of the microneedle and the backside channels, evaporation at the distal opening above the reservoir maintained the pressure gradient allowing for a continuous capillary draw of the fluid. Nonetheless, no calibration of the system against glucose concentration was reported.

The first report on solid glass microneedles was given by Wang et al. in 2005,[72] which demonstrated in vivo extraction of ISF for ex situ glucose detection (**Figure 6**). The use of

glass for microneedles was motivated by the peculiarities of this material, which is physiologically inert, sterile, and transparent. Moreover, conventional glass needles have largely been used in intracellular recording as well as microinjection and patch clamping applications, due to the low cost and easy fabrication.[73] Glass single-needles were fabricated by means of a programmable thermal micropipette puller using borosilicate glass capillary tubing (outer diameter of 1.5 mm, inner diameter of 0.86–1.10 mm). Demonstration of multi-needles array fabrication was given through the mechanical assembling of seven single-needles, as shown in Figure 6a. Microneedles featured a tip radius of 15–40 µm with a cone angle of 20–30°. Although the needles had a hollow bore, the needle tips were sealed by glass melting in order to increase their mechanical strength. Glass microneedles were successfully used to penetrate the skin for a depth of 700–1500 µm and extract dermal ISF from both the back of anesthetized hairless rats and the forearm of adult human volunteers (Figure 6b). In particular, a 1-cm^2-large area of skin was pierced to make 7 to 10 holes using either repeated insertions of a single microneedle or a single insertion of a multi-needle array. A cone-shaped geometry of microneedle-created holes with radii of 80–250 µm and depths of 700–1500 µm, similar dimensions to those of the needles themselves, was confirmed by different analyses. ISF was extracted by applying a negative pressure of 200–500 mm Hg (using a vacuum rotary pump) to the punctured skin for either 2–10 min in animal tests or 5–20 min in human tests. Ultimately, ISF drops were collected from the treated skin through the use of glucose test strips, which were immediately analyzed to assess the glucose concentration. ISF volumes extracted were typically 1–10 µL, which were sufficient to measure glucose concentration through commercially available devices. As controls for ISF glucose levels, blood was also collected from both rats and human subjects by lateral tail vein laceration and fingertip puncturing, respectively, and similarly analyzed. By comparing measured ISF and blood glucose levels, a tight correlation with a linear dependence was found for both animals and humans, with 95% of measurements made in rats and 100% of measurements made in humans falling within the A+B region of the Clarke Error Grid analysis[74] (Figure 6c). Finally, a kinetic study was carried out to monitor glucose levels both in ISF and in blood at time intervals of 20 min, after intraperitoneal injection of 1U of insulin (Figure 6d). Measurements showed a rapid decrease of the glucose level in blood after insulin injection, closely followed by microneedle-extracted ISF glucose level, with no significant time lag given the 20 min time resolution, thus demonstrating that glass microneedles could be used for painless glucose monitoring in dermal ISF extracted in a minimally invasive manner.

Using a similar approach, an array of solid microneedles was used to extract ISF in a minimally invasive manner and to subsequently monitor postprandial hyperglycemia ex situ.[75] To accomplish this goal, the glucose area under the curve (AUC) was measured as accumulated ISF glucose (IG) with simultaneous calibration with sodium ions (Na^+) used as an internal standard. The microneedle array was made of polycarbonate (PC), and featured 305 needles with length of 300 µm over an area of 50 mm^2. The microneedle array was stamped on the forearm skin as a pretreatment to form micropores for enhancing ISF extraction. A handheld spring-activated applicator was used to apply the microneedle array to the forearm skin at an application speed of 6 m s^{-1}, which resulted in a penetration depth of approximately 100 µm. A reservoir consisting of a hydrogel patch containing polyvinyl alcohol (PVA) with 2% KCl solvent was then placed on the pretreated area of the skin to accumulate ISF for a specific time period. No additional force was needed to extract ISF from the skin, except passive diffusion and osmotic pressure. The glucose AUC during the collection time period (from 1 to 3 h with step of 1 h) was measured by analyzing glucose levels in the ISF accumulated in the reservoir. Na^+ were chosen as an internal standard for calibration being their concentrations in both ISF and blood stable over time (i.e., not dependent on time) and comparable among different individuals. Hydrogels were immersed overnight in 5 mL of pure water to extract glucose and Na^+. Glucose levels were obtained by mixing 0.1 mL of the sample solution with 0.1 mL of glucose analysis reagent, and measuring the fluorescence intensity of the Amplex Red dye after incubation for 60 min. Na^+ levels were analyzed using an ion chromatography system. Glucose concentration was confirmed by blood measurements carried out every 15 min for 3 h with a commercial glucose meter used as control. Firstly, the correlation between glucose and Na^+ levels was evaluated in 16 subjects (healthy volunteers) with stable blood glucose (BG) levels during fasting. A high correlation was observed between glucose and Na^+ levels when BG levels were stable ($R = 0.87$), indicating that Na^+ were a good internal standard for calibration. Furthermore, BG and IG time courses were evaluated in three subjects to investigate whether IG variation was coupled with BG variation, before and after a meal. It was observed that IG was closely correlated with BG within the limited range of glucose variations in healthy volunteers, thus indicating that IG was an adequate substitute for BG. Finally, the accuracy of glucose AUC measurements in ISF extracted via microneedles was evaluated several hours after a meal in 30 healthy subjects. A strong correlation ($R = 0.92$) between IG-AUC and BG-AUC after a meal was observed, thus indicating that IG-AUC was a good substitute for BG-AUC and a potentially useful index for postprandial glycemic excursions.

As a next step, the same group evaluated the usefulness of ISF extraction via microneedles for monitoring IG-AUC through the above-described approach by comparing data obtained from subjects with (37) and without (10) diabetes with the oral glucose tolerance tests (OGTTs) being performed as part of medical therapy.[76] Plasma glucose (PG) levels were measured every 30 min for 2 h by means of a commercial glucose meter and used to calculate PG-AUC as reference. IG-AUC strongly correlated with PG-AUC ($R = 0.93$) over a wide range (227–675 mg h dL^{-1}), with correlation being independent of glucose tolerance classification. Further, the level of correlation between PG peak and predicted IG-AUC was also good ($R = 0.86$) and independent of the PG peak level. Interestingly, results from a patient questionnaire on pain caused by using either microneedles or commercial self-monitoring blood glucose systems confirmed that the former were retained painless from 97% of subjects (against 45% of the latter).

One year later, the same group further corroborated the efficacy of measuring the glucose AUC using minimally invasive ISF extraction technology (MIET) via microneedles on

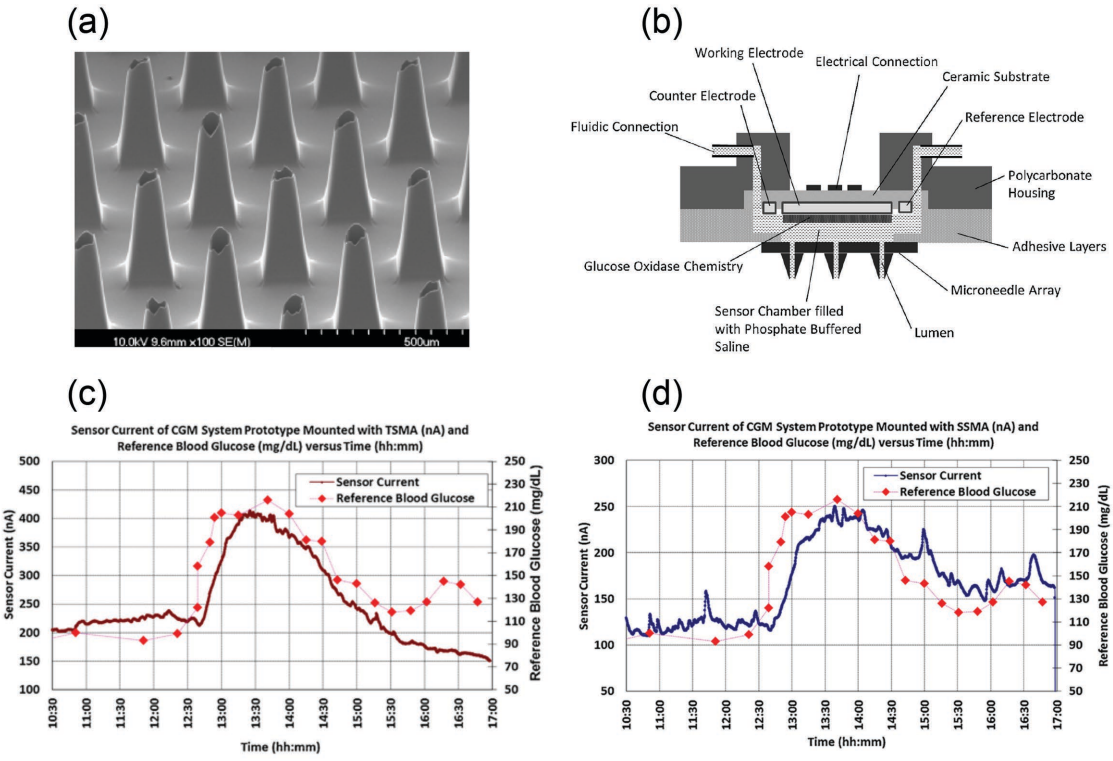

Figure 7. An ISF-targeting CGM system based on tapered silicon microneedles. a) SEM image of TSMA. b) Schematic of the CGM system prototype, showing its main components. c,d) In vivo continuous measurements of ISF glucose over time with two CGM system prototypes making use of tapered and straight silicon microneedle arrays, respectively. Reproduced with permission.[37] Copyright 2013, Elsevier.

50 patients scheduled to undergo OGTT.[77] Both feasibility and effectiveness of the system were investigated in view of developing a new screening tool for glucose intolerance. The data obtained were consistent with those achieved in,[76] thus suggesting that glucose AUC measurements using MIET could be useful for screening of glucose intolerance.

In 2013, Chua et al.[37] reported the use of hollow silicon microneedle arrays for in vivo minimally invasive continuous glucose monitoring (CGM) (**Figure 7**). Minimally invasive CGM systems based on microneedles able to penetrate a few hundred micrometers below the skin have been predicted to be significantly less painful, infection-free and more accurate with respect to implantable CGM systems available on the market.[78–80] Straight silicon microneedle arrays (SSMAs) and tapered silicon microneedle arrays (TSMAs) were fabricated using standard silicon micromachining techniques (Figure 7a). TSMAs and SSMAs shared similar DRIE steps, though TSMAs were sharpened via HNA (hydrofluoric acid/nitric acid/acetic acid) etching,[71] whereas SSMAs were sharpened via a mask depletion process using DRIE.[81] Microneedle heights were about 325 µm and 350 µm and pitches were 400 µm and 450 µm for SSMAs and TSMAs, respectively. Microneedle lumen was about 50 µm × 50 µm in size. A CGM system prototype was achieved by assembling an electrochemical glucose sensor and a hollow microneedle array on opposite sides of a glucose chamber through the use of a PC housing[82,83] (Figure 7b). The glucose sensor consisted of screen-printed electrodes (Pt working electrode, Ag/Ag Cl reference and counter electrodes), with the surface of the working electrode (about 6 mm × 6 mm) coated with GOx chemistry formulation. The CGM system prototype was loaded into a spring-based mechanical applicator that allowed application of the needles to the human skin at an impact velocity of about 10 m s^{-1}. After application of the sensor/microneedle assembly to the skin, the sensor chamber was pumped with PBS solution to allow the glucose to diffuse from the ISF into the sensor chamber via the microneedle lumens. The glucose sensor was then electrically connected to an external biasing/acquisition circuit. In vivo experiments were carried out on human subjects fasted for 2 h before taking a meal to increase the glucose concentration in blood (Figure 7c,d). The biosensor current was continuously measured over time for 6.5 h, at a sampling frequency of 1 Hz. A commercial glucose meter was used to monitor glucose concentration in blood as control. The sensor currents of both the CGM system prototypes appeared to trace the reference blood glucose values (between 90 and 220 mg dL^{-1}) reasonably well. However, the CGM system prototype making use of SSMAs registered a lower sensor current (between 100 and 250 nA) as compared to that using TSMAs (200–400 nA). A qualitative in vivo evaluation of both TSMAs and SSMAs penetration capabilities, carried out by staining the skin with 2% methylene blue solution after the microneedle arrays were removed, highlighted that TSMAs mostly created mode-I planar cracks when inserted into the skin, whereas SSMAs preferentially created mode-II ring cracks.[84] It implied that the SSMAs lumens were more likely to be occluded by the displaced skin material than the TSMAs lumens, thus possibly explaining the lower sensor current of SSMAs (maximum at 250 nA) as compared to that of TSMAs (maximum at 400 nA).

This microneedle-based CGM system equipped with TSMA was later used to carry out a clinical trial on diabetic patients.[85] Ten adult subjects with insulin-dependent diabetes and average age of about 61 years (range 33–78 years) were recruited. Each subject wore four sensor-microneedle systems that were applied to both the upper arm and forearm for either 48 h (6 out of 10 subjects) or 72 h (4 out of 10 subjects). Subjects reported to the study site daily for comparative finger stick glucose measurements, taken every 20 min with a commercial glucose meter. Glucose excursions into both hypo- and hyper-glycemic ranges were generated by manipulating insulin and diet. The microneedle-based CGM systems were firstly calibrated after an initial 2 h warm-up period using a reference finger stick glucose value, and then once daily with the morning finger stick glucose value. A lag-time of 17 min minimizing error between finger stick measurements and CGM system readings was determined by measurements taken on nondiabetic volunteers and applied to clinical data from the diabetic subjects. Good agreement was achieved between the microneedle-based CGM data and finger stick glucose values, with 74.6% of paired points located in the A-region of the Clarke Error Grid and 98.4% in the A+B region. The mean relative difference (MRD) was 5% with an overall mean absolute relative difference (MARD) of 15%, indicating a low level of both systematic and random errors in the dataset (a total of 1396 paired points were obtained from 37 devices). Skin irritation upon removal of the sensor-microneedle systems was scored using a Draize scale (from 0 to 4, with higher numbers meaning more severe irritations). Average erythema and edema scores were 1.54 and 0.06, respectively, with skin irritation resolved completely without treatment in several days.

More recently, Valdés-Ramírez et al.[86] realized a microneedle-based self-powered biofuel-cell (BFC) sensor for subdermal glucose monitoring (**Figure 8**). According to the general definition given by Bullen et al.,[87] BFCs are "devices capable of directly transforming chemical to electrical energy via electrochemical reactions involving biochemical pathways". BFCs are very attracting for on-body applications since they offer an approach to develop an autonomous energy supply (thus eliminating the need for external power source) for medical devices by harvesting energy from body fluids. Within this aim, microneedle-based BFCs offer considerable promises as self-powered biosensors capable of harvesting biochemical energy from subdermal fluids and providing power signals proportional to the concentration of the analyte (i.e., the fuel) of

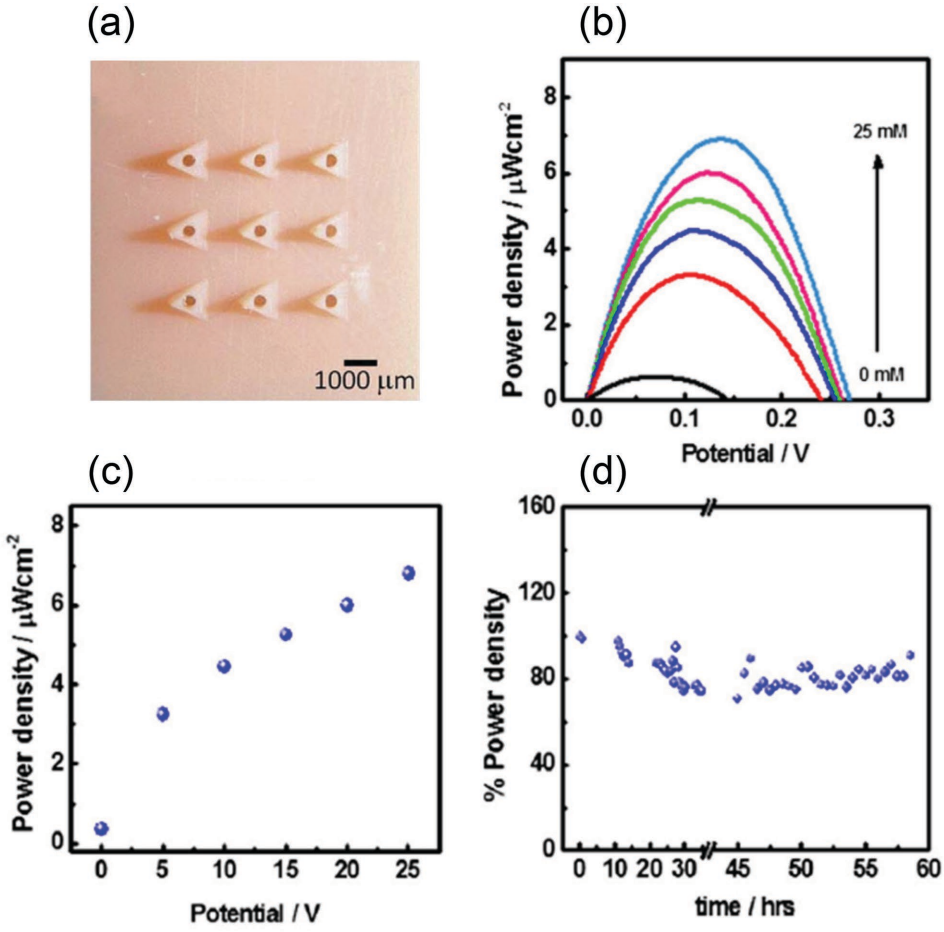

Figure 8. A microneedle-based self-powered BFC sensor for subdermal glucose monitoring. a) Optical micrograph of a 3 × 3 square microneedle array. b) Power density versus supply voltage of the BFC sensor for different glucose concentrations in artificial ISF. c) Calibration curve (maximum power density value versus glucose concentration) of the BFC sensor. d) Stability of the microneedle-based BFC sensor for 60 h of continuous operation. Reproduced with permission.[86] Copyright 2014, Elsevier.

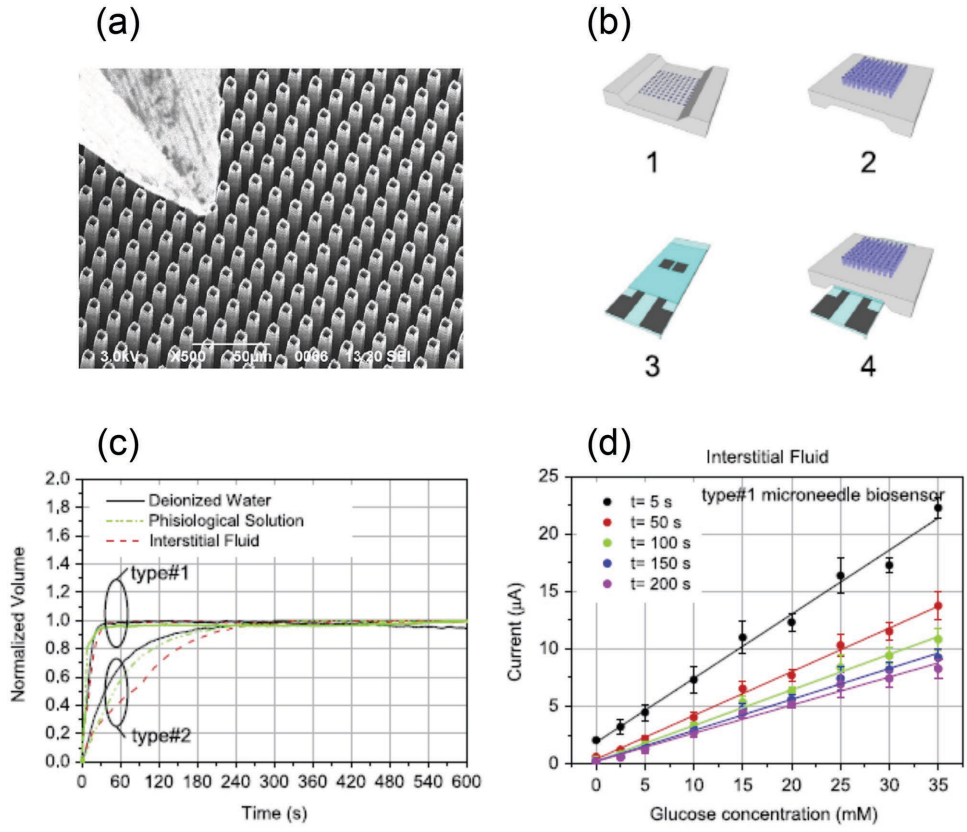

Figure 9. A self-powered capillary-driven microneedle-based biosensor for glycaemia measurements in ISF. a) SEM image of a type#1 microneedle array with an insulin needle on top of the array for comparison. b) Schematic of the capillary-driven microneedle-based biosensor. c) Time-resolved capillary-uptake curves of different liquids, including ISF, for type#1 and type#2 microneedle chips. d) Calibration curves of type#1 capillary-driven microneedle biosensors for increasing glucose concentrations (0–35 mM) in ISF solutions at different sampling times. Reproduced with permission.[91] Copyright 2015, Elsevier.

interest.[88,89] The microneedle-based self-powered BFC glucose sensor was realized through the integration of a BFC carbon-paste bioanode and cathode into a hollow microneedle array (Figure 8a). The hollow microneedles (3 × 3 array) were similar to those reported in.[90] The bioanode was obtained by mixing carbon paste (87%) with the enzyme (10% GOx) and mediator (3% tetrathiafulvalene, TTF), whereas the cathode was obtained by mixing the carbon paste with Pt black (1:1 weight ratio). The prepared carbon paste-GOx-TTF bioanode and the carbon paste-Pt black cathode were finally extruded into six hollow microneedles of the array, with one row of three microneedles working as bioanode and one row as cathode. An Ag/AgCl reference electrode and a Pt wire counter electrode completed the three-electrode system for the electrochemical characterization. In vitro characterization of the microneedle-based BFC sensor for subdermal glucose monitoring was carried out by using artificial ISF[27] with glucose concentration in the range 0–25 mM (Figure 8b). Power density as a function of glucose concentration showed a linear behavior over the whole range 0–25 mM (Figure 8c), thus indicating that suitable glucose measurements addressing both hypoglycemia and hyperglycemia could be performed. In particular, a low power density of 0.4 μW cm^{-2} was obtained for the blank solution (0 mM glucose), whereas higher power densities of 3–5 μW cm^{-2} were observed over the normal glucose range (5–10 mM glucose) with a maximum value of 7 μW cm^{-2} at 25 mM glucose. The stability of the microneedle-based BFC sensor during a continuous 60 h period monitoring was further evaluated in artificial ISF containing 10 mM glucose and 20.6 mg mL^{-1} BSA (Figure 8d). Around 75% of the original power density was retained after the 60 h time period monitoring, thus indicating a good resistance of the system to biofouling effects. Selectivity of the microneedle-based BFC glucose sensor was then assessed by recording the glucose power signal in the presence of common electrochemical interferences (i.e., ACT, AA, UA, and lactic acid), under physiological conditions. No significant effects on the glucose power-density signal were observed for any of the tested interferences.

A recent work on the development of self-powered microneedle-based biosensors was reported by Strambini et al.,[91] which described the self-powered uptake of ISF by using tiny SiO_2 hollow microneedles as well as their in vitro use for glucose detection in ISF by combining the microneedle chip with an enzymatic glucose sensor (**Figure 9**). The microneedle chip consisted of a silicon die integrating a two-dimensional array of hollow SiO_2 (thickness of 1 μm) needles protruding from the front-side of the chip for about 100 μm (Figure 9a). The needles were, in turn, connected with a reservoir grooved on the back-side of the chip through a 200-μm-long internal channel. Two arrays of microneedles with different diameters and spatial periods were fabricated (refer to Strambini et al.[92] for

details) and tested, namely type#1 chips with period $p = 16$ µm, external and internal diameter $d_e = 9$ µm and $d_i = 7$ µm, respectively, and type#2 chips with $p = 10$ µm, $d_e = 6$ µm, $d_i = 4$ µm. Both type#1 and type#2 chips were used to quantify the capability of such microneedles to draw fluids (i.e., deionized water (DIW), standard physiological solution (PSS), and synthetic ISF solution) and collect them into the integrated reservoir by only capillary-action, that is without the use of external pumps (Figure 9c). Type#1 needles were found to be considerably faster (a factor of 10 for ISF) than type#2 needles for each of the tested liquids. The results demonstrated that fast (i.e., uptake rates up to 1 µL s^{-1}) and pump-free uptake of biological fluids could be carried out with high efficiency, accuracy, and reproducibility by exploiting capillarity in tiny (borehole down to 4 µm) and densely packed (up to 1×10^6 needles cm^{-2}) microneedles. In order to realize microneedle-based biosensors, both type#1 and type#2 chips were coupled with an enzymatic glucose biosensor, which was placed into the reservoir integrated on the back-side of the needle chips (Figure 9b). The biosensor electrodes were fabricated through a screen-printed process using a carbon-based polymeric ink to realize the working and counter electrodes, and an insulating ink to cover the electrode surfaces and to define the electrode working area. After fabrication, the electrodes were modified with a layer made of carboxymethylcellulose (CMC), the glucose-specific enzyme GOx and potassium ferricyanide ($K_3[Fe(CN)_6]$). Microneedle-based glucose biosensors (both type#1 and type#2) were characterized in vitro by chronoamperometry, using synthetic ISF solutions[27] with glucose concentrations in the range 0–35 mM (0–630 mg dL^{-1}), which were collected by capillary-action through the needles (Figure 9d). A stand-alone glucose biosensor (i.e., without needles) was used as control. Performance of self-powered microneedle-based biosensors for glucose measurements in ISF was evaluated for different sampling times from 5 to 200 s (10 s steps) through quantification of several analytical parameters (i.e., accuracy, linearity, reproducibility, sensitivity, and resolution). Good linearity was obtained over the whole range of concentrations for any sampling time. The best performance (in terms of compromise between sensitivity, accuracy, and reproducibility) of self-powered microneedle-based glucose biosensors was obtained at a sampling time of 30 s, for which type#1 (type#2) biosensor accuracy was within ±20% of the actual glucose level for 96% (92%) of measures carried out on ISF solutions over the whole range 0–35 mM (0–630 mg dL^{-1}) of glucose. The results obtained complied with FDA standards, according to which above 75 mg dL^{-1} (4.2 mM), 95% of measurements must be within ±20% of the actual glucose level.[93] Furthermore, reproducibility of 8.56% and 8.74%, sensitivity of 0.43 µA mM^{-1} and 0.46 µA mM^{-1}, and LODs of 0.3 mM and 0.9 mM were reported for type#1 and type#2 biosensors, respectively. Control measurements with stand-alone biosensors yielded analytical parameters that were in good agreement with those of microneedle-based biosensors.

3.2. Biomarker Detection

Microneedles have recently been proposed as point-of-care (PoC) devices for the emerging field of molecular diagnostics.[94] Today, common diagnostic assays for the detection of biomarkers are based on intravenous blood samples drawn via needle/syringe methods, which involve handling and transport of contaminated blood to specific laboratories, thus requiring time, high resource settings and costs, as well as trained laboratory staff.[95] Furthermore, the use of invasive tools, such as hypodermic needles, makes such an approach unsuitable for frequent monitoring of patients.[96]

In their pioneering work, Corrie et al.[97] proposed, for the first time, the use of tiny and sharp silicon microneedles, termed microprojection arrays (MPAs), for selective transdermal extraction of biomarkers directly from serum-rich fluids in the skin epithelia (**Figure 10**). MPAs were synthetized from (100) silicon using a DRIE–based process, and then coated with a thin film of gold (Figure 10a). The density and length of gold-coated needles were 20 000 cm^{-2} and 65 µm, respectively, with base diameter of 25 µm and sub-micrometer sharp tips. The needles were successfully applied to mouse ear skin at constant velocity of a few m s^{-1},[33] achieving reproducible penetration in the upper dermis (19 ± 5 µm), which is rich in capillary blood.[98] As-fabricated and polyethylene glycol (PEG)-modified MPAs were tested in vivo to evaluate the effectiveness of such needles to extract systemic biomarkers present in skin fluid after penetrating into the dermis (Figure 10b,c). PEG grafting to gold-coated MPAs was used to both reduce non-specific protein adsorption and provide an anchor for capturing protein attachment. Both as-fabricated and PEG-modified MPAs were applied for 10 min to mice ear skin, 21 days after their vaccination by intramuscular injection with FluVax (a commercial trivalent influenza vaccine). The resulting anti-FluVax IgG (AF-IgG) level was measured using an enzyme-linked immunosorbent assay (ELISA) method, both for MPA-extracted fluid and needle-extracted blood, which confirmed that AF-IgG levels on the two samples were comparable. Moreover, a >90% reduction in non-specific protein adsorption with PEG-coated MPAs was measured. PEG-modified MPAs were then functionalized with AF-IgG capture proteins (termed PEG-FLU MPAs) to investigate, through the use of a MPA-ELISA assay, specific binding of AF-IgG both in vitro in 10% mouse serum and in vivo applying the device to mouse ear skin for 10 min. MPAs modified with ovalbumin (OVA) grafted on PEG, termed PEG-OVA, were used as control. PEG-FLU MPAs extracted significantly more AF-IgG, both for in vitro and in vivo testing, with respect to PEG-OVA MPAs. In particular, PEG-FLU MPAs extracted significantly higher AF-IgG from immunized mice than from naïve (S/N = 16) thus highlighting a high analytical specificity, whereas no significant difference between immunized and naïve mice was found for PEG-OVA and PEG-coated MPAs. PEG-FLU MPAs also showed significantly higher signals in comparison to both as-fabricated and PEG-modified MPAs. Nonetheless, skin applications yielded a different fluorescence distribution along the microprojection in comparison to the serum incubation results, as analyzed by confocal microscopy. In particular, skin application resulted in a tip-specific fluorescent signal, whereas serum incubation resulted in a relatively even distribution of the same signal. Finally, the analytical sensitivity of MPAs was evaluated by comparing AF-IgG levels measured at given time points using MPA-ELISA with conventional ELISA. Both methods measured statistically

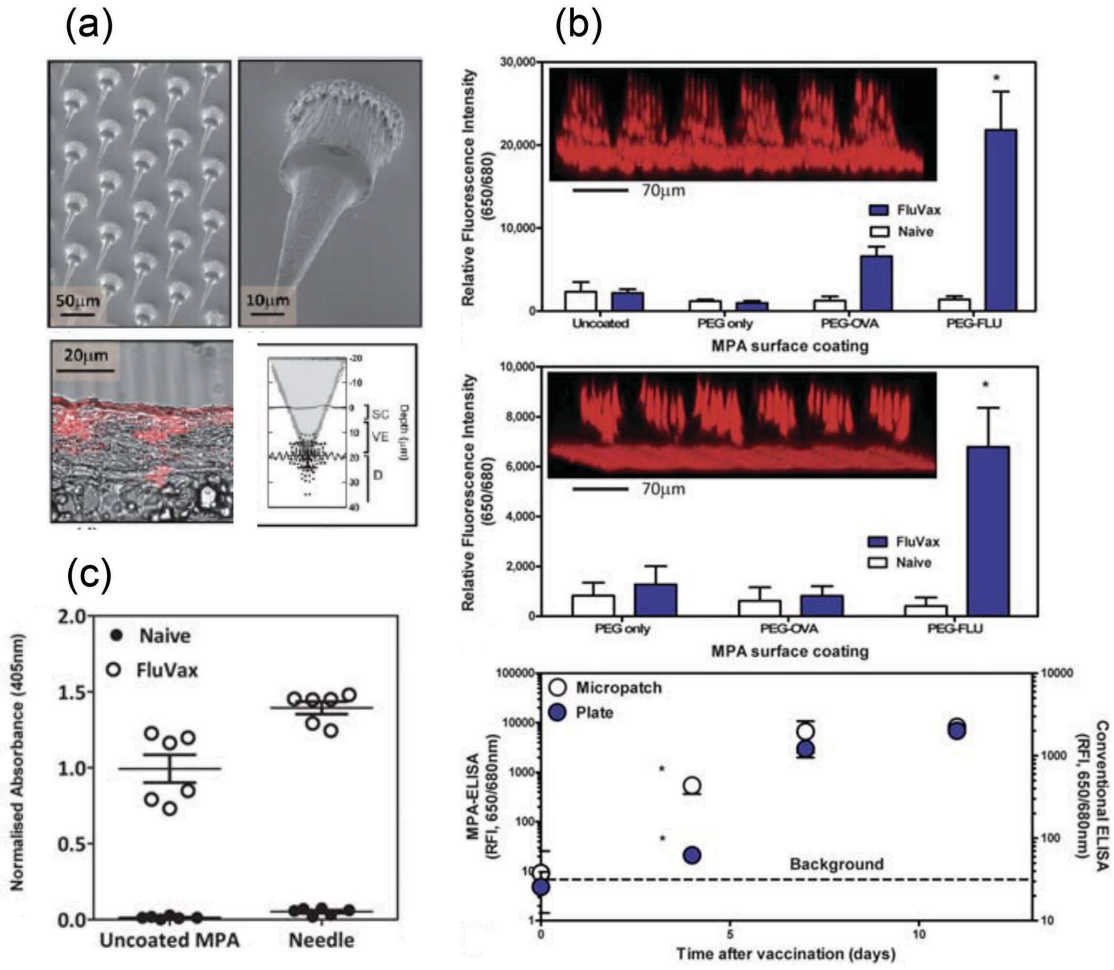

Figure 10. MPAs for intradermal biomarker capture. a) SEM images of a highly dense array of microprojections (top), and results of dermal penetration obtained after application of fluorescently coated MPAs to mouse ear skin (bottom). b) Fluorescent MPA-ELISA results for AF-IgG detection using MPAs with different coatings, in serum (top) and in skin (center), and comparison between MPA-ELISA and standard ELISA involving serum analysis after needle extraction of whole blood (bottom). c) In vivo AF-IgG biomarker detection with either MPAs or a standard needle in FluVax-vaccinated mice. Reproduced with permission.[97] Copyright 2010, Royal Society of Chemistry.

detectable levels (30 ng mL^{-1}) of AF-IgG 4 days after mice vaccination, indicating equivalent analytical sensitivities between the two techniques.

On the basis of these results, in 2012 Muller et al.[99] exploited silicon MPAs with higher lengths for the in vivo capture of viral nonstructural protein 1 (NS1) used as an early marker of dengue virus infection (**Figure 11**). Dengue virus is an important human pathogen that is spread through the bite of infected *Aedes aegypti* mosquitoes and that causes about 100 million infections each year across the tropical belt, with half of the world's population at risk of infection.[100] NS1 is secreted from infected cells from the onset of disease symptoms with as much as 50 μg mL^{-1} being reported 12 days post disease onset.[101]

MPAs with different lengths, namely 110 and 260 μm, and different shape designs, namely "cone-on-cylinder" and "bullet", were produced through a DRIE-based process followed by gold coating. PEG coating of the as-fabricated MPAs was used to allow for captured antibodies to be covalently immobilized to either amine or carboxylic acid functional groups via *N*-(3-dimethylaminopropyl)-*N*'-ethylcarbodiimide hydrochloride (EDC)/*N*-hydroxy succinimide (NHS) chemistry as well as to create an antifouling layer to significantly reduce nonspecific binding of proteins to the needle surface. Assay investigation and development for high capture efficiencies of antigens from skin using MPAs was optimized in vitro by detection of total IgG through ELISA, which was used as positive control, and by comparing MPA devices with Nunc maxisorp plate surfaces. A goat antimouse IgG Fc specific capture antibody was covalently attached to PEG-coated MPAs and used to bind mouse IgG. Captured IgG was then detected by a goat antimouse IgG Fab specific horseradish peroxidase (HRP) conjugate antibody. After taking into account the difference in surface area, no significant changes in titration curves obtained by absorbance measurements at 450 nm were observed for MPAs and Nunc plate surfaces. For in vitro detection of the dengue virus antigen NS1, a similar protocol was used with NS1 being captured with an anti-NS1 monoclonal antibody and detected by an anti-NS1 HRP conjugate antibody. After normalization of fluorescent signals for the lower surface area of the MPA, a striking difference between Nunc plate surfaces and MPA was evident.

Adv. Healthcare Mater. **2015**,
DOI: 10.1002/adhm.201500450

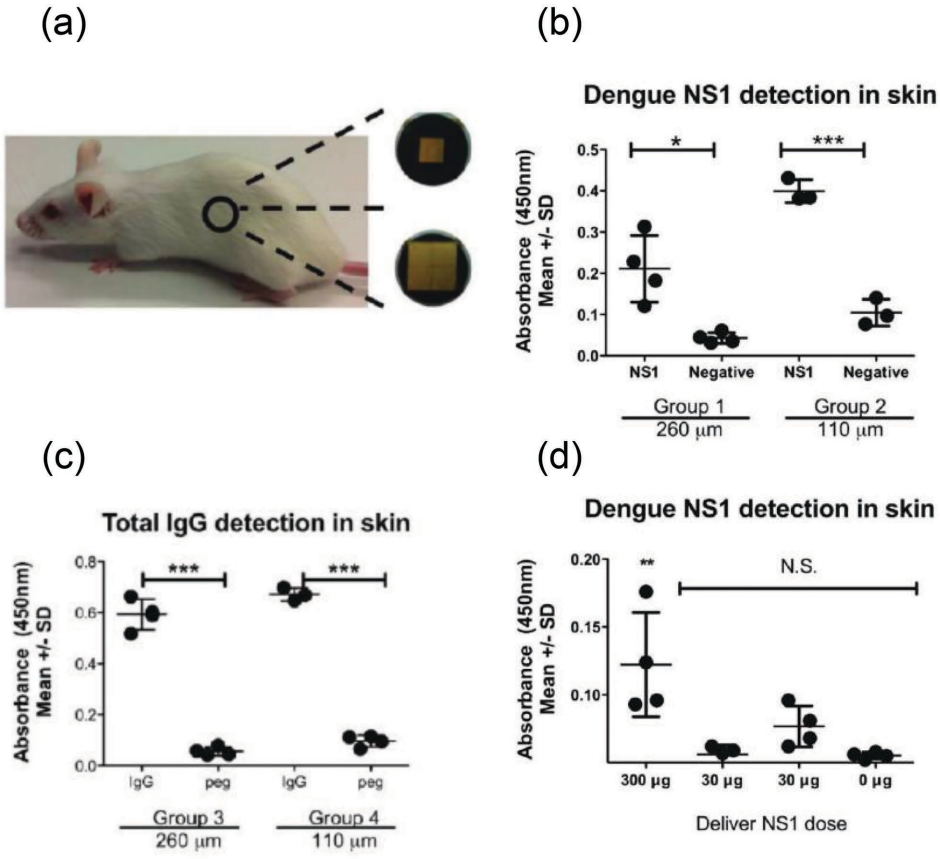

Figure 11. MPAs for the extraction of the dengue Virus NS1 protein. a) Location of the flank skin of live mice for MPA application. b) NS1 extracted from skin fluid by MPAs featuring two different lengths (110 and 260 μm). c) IgG extracted from skin fluid by MPAs featuring two different lengths (110 and 260 μm). d) Lowest detectable level of NS1 in skin using MPAs with lengths of 110 μm. Reproduced with permission.[99] Copyright 2012, American Chemical Society.

On the Nunc plate, dilution of NS1 into either a simple (e.g., BSA only) or complex (e.g., plasma or serum) protein source had no significant effect on the titration curves. Conversely, better results were obtained on MPA surfaces using BSA with respect to plasma and serum, which highlighted a titration curve featuring saturation signals similar to Nunc plates but with a lower initial slope.

In vivo extraction of circulating antigens with MPA was carried out from the flank skin of live mice using the in vitro established protocols (Figure 11a). Based on penetration depth analysis, which was performed by coating the microneedles with fluorescent nanospheres followed by application to the skin, penetration depths were evaluated to be 79 ± 14 μm and 119 ± 15 μm for 110-μm-long and 260-μm-long needles, respectively. Afterwards, application of NS1- and IgG-specific MPAs to the skin of live mice was carried out after intravenous injection of NS1 protein as a pseudomodel of dengue virus infection. Flank skin was chosen over ear skin due to the increased signal resulting from the former. Both NS1 and total IgG in mice were successfully detected with respect to negative controls, regardless of projection length (Figure 11b,c). Surprisingly, after normalizing for the differences in total surface area, the 110-long-MPAs yielded moderately higher extraction efficiency in comparison to the 260-long-MPAs, probably due to the more successful shape of the former in capturing markers in the skin. Although the detection limit was not determined in this study, NS1 was detected in vivo at a minimum level of 8 μg mL^{-1} (Figure 11d), which was consistent with levels detected in clinical serum/plasma samples.[102]

Lower and more variable fluorescent signals across MPA device surfaces when applied directly to skin, with respect to serum exposure from the same animals, were successfully addressed by Bhargav et al.,[103] which optimized the biochemical assay in terms of both the underlying surface chemistry and probe immobilization chemistry to increase target capture efficiency and improve the quantitative potential of this technology. Gold coated silicon MPAs (cone-shaped cylinder projections with length of 100 μm) were fabricated through a DRIE-based process followed by standard chrome/gold evaporation (referred to as Au-MPAs) and PEG coating (referred to as PEG-Au MPAs). A fluorescently labeled PEG layer (referred to as FITC-PEG-SH) was specifically used to investigate monolayer uniformity across a 4 × 4 mm MPA surface after coating by means of a flat-bed confocal laser scanner. Across the entire PEG-Au MPAs the coefficient of variation CV% (defined as the ratio of standard deviation and mean, expressed as a percentage) of the fluorescent signal was 19.2 ± 1.2%, though much of the variation in the level of fluorescence could be explained by the

presence of the projections. After preparation of the PEG-Au MPAs, the arrays were firstly placed in an equimolar mixture of EDC and NHS in 2-(*N*-morpholino)ethanesulfonic acid (MES) buffer and then suspended in protein solution containing OVA in PBS, thus obtaining OVA-immobilized MPAs (referred to as OVA PEG-Au MPAs). α-OVA-IgG antibodies to be detected were obtained by sampling blood serum of OVA-vaccinated mice 21 days after vaccination. The Alexa Fluor 647-labeled F(ab)2 fragment of goat antimouse IgG (referred to as AF647-Det-IgG) was used to determine the relative amount of target antibody captured by OVA PEG-Au MPAs. Experiments were specifically carried out to investigate the nature of the OVA-PEG interaction in the presence or absence of EDC/NHS as well as the subsequent affinity interactions in the indirect model ELISA system. Quantitative results suggested that the protein immobilization procedure accounted for a significant variation in signal intensity across the MPA surface (CV% of fluorescent signal 533 ± 447%), with respect to other steps of the assay. In order to address this issue, the protein immobilization conditions in the EDC/NHS chemistry were investigated by varying pH, time t and temperature T, and assessing the response by measuring the degree of bound AF647-OVA. Following optimization of the probe immobilization (referred to as "optimized conditions", pH = 4.5, t = 960 min, T = 37 °C), a 60-fold increase in the fluorescent signal together with an improved degree of the fluorescent signal uniformity across the MPA surfaces (CV% = 36 ± 8%) was achieved, with respect to controls. Both in vivo (i.e., application of MPAs to the flank skin of live OVA-vaccinated mice) and in vitro (i.e., in serum from the same animals, diluted 10% in PBS containing 0.02% Tween 20 surfactant) tests using OVA PEG-Au MPAs under optimized protein conditions were carried out followed by subsequent AF647-Det-IgG binding and fluorescence analysis. For both in vivo and in vitro assays, the optimized protein coupling conditions yielded significantly higher AF647-Det-IgG signals in vaccinated mice with respect to controls, increasing by 18-fold and 140-fold, respectively.

In order to investigate the effect of penetration depth and application time on early circulating biomarker detection using microneedles, Coffey et al.[104] fabricated three silicon MPAs, by DRIE-based process and subsequent chrome/gold coating, with the same density (i.e., 20 000 cm^{-2}) but different lengths (i.e., 40, 100, and 190 µm). For penetration tests, MPAs were dry coated with yellow-green fluorescent nanoparticles (diameters of 0.2 µm) hosted in a methylcellulose matrix, this latter dissolving once wetted in the skin allowing for the visualization of penetration tracks. MPAs were then applied in vivo to anaesthetized mice at an application velocity of 3.1 m s^{-1} using a spring loaded applicator device designed for murine abdominal skin. Penetration depths were quantified through confocal microscopy following in vivo MPA application and histological sectioning by measuring the fluorescent signals from the nanosphere tracer that remained in the skin after MPA removal. Penetration depths of 27 ± 9 µm, 78 ± 14 µm, and 153 ± 30 µm were found for the 40, 100, and 190 µm long MPAs, respectively. In vivo investigation of anti-FluVax-IgG biomarker capture in abdominal skin as a function of the penetration depth was carried out over a single 10 min application, during peak anti-FluVax-IgG levels post vaccination. Mice were immunized with FluVax vaccine 2009 by intramuscular injection at least three weeks prior to application of surface-modified MPAs. As-fabricated MPAs were firstly coated with PEG, then immobilization of hemagglutinin proteins on projection surface was performed by immersing PEG-coated MPAs in a solution of FluVax vaccine 2009. Using the three different microneedle lengths, a 4-fold increase in the anti-FluVax-IgG extraction yield was observed, moving from 40-µm-long MPAs (which mainly penetrated only the epidermal layer and extracted a marginally significant amount of biomarker in comparison to naïve mice controls) to 190-µm-long MPAs (which penetrated the deep dermal layer). In vivo investigation of anti-FluVax-IgG biomarker capture kinetics as a function of application time was carried out during peak anti-FluVax-IgG levels post vaccination using the 100-µm-long MPAs. Both "rapid" (namely, 1, 5, 10, and 20 min) and "long-term" (namely, 20 min, 1, 2, 4, 6, 9, and 24 h) application times were investigated. Biomarker capture over time was statistically significant at 10 and 20 min (rapid application), with a 6-fold peak increase after 6 h (long-term application). No further increase was noted up to 24 h, suggesting probable saturation of the capture surface with anti-FluVax-IgG. A mild erythema upon removal of the MPAs regardless the application time was observed, although this effect cleared up over the following 24–48 h. In an effort to improve MPA detection and diagnostic sensitivity, a combined in vivo study was finally carried out to simultaneously investigate the effect of both penetration depth and application time. Both 100-µm-long and 190-µm-long MPAs were applied for 10 min and 6 h to detect anti-FluVax-IgG in the skin over days 4–6 following immunization. Comparison of capture yields suggested that the 100-µm-long MPAs did not show significant biomarker capture neither for shorter nor for longer times (only 3/5 replicates returned a positive result on day 6 after 6 h application). Conversely, the 190-µm-long MPAs exhibited significant biomarker capture (over the cut-off level for all the replicates) at day 6 for 10 min application time and across all days 4–6 for 6 h application time, comparable to biomarker levels measured using a traditional gold standard plate ELISA.

Although silicon has traditionally been used as a material for microneedle fabrication, polymers have also been taken into consideration recently thanks to their significant advantages over silicon in terms of biocompatibility, biodegradability, and cost-effectiveness.[14,105] Very recently, a first report on surface-modified PC MPAs for the capture of specific biomarkers from live mice either in vitro (i.e., using serum) or in vivo (i.e., in the animal flank skin) was described[106] (**Figure 12**). PC-MPAs were fabricated by standard compression molding using a PDMS negative mold of a silicon MPA master, which was fabricated as reported by Jenkins et al.[107] (Figure 12a). Comparison between silicon-MPAs and PC-MPAs showed projection lengths of ≈80 µm with diameters of ≈40 µm in both cases, albeit the latter was considerably less sharp than the former. Nonetheless, penetration depths of silicon-MPAs and PC-MPAs into the mouse flank skin were not significantly different (Figure 12b,c). PC-MPAs were therefore subjected to a surface-modification firstly in nitric acid to insert aromatic nitro groups (-NO_2) into the benzene rings and subsequently in sodium borohydride to reduce -NO_2 groups to amine groups (-NH_2). Introducing amine functional groups into the PC surface via electrophilic

Adv. Healthcare Mater. **2015**,
DOI: 10.1002/adhm.201500450

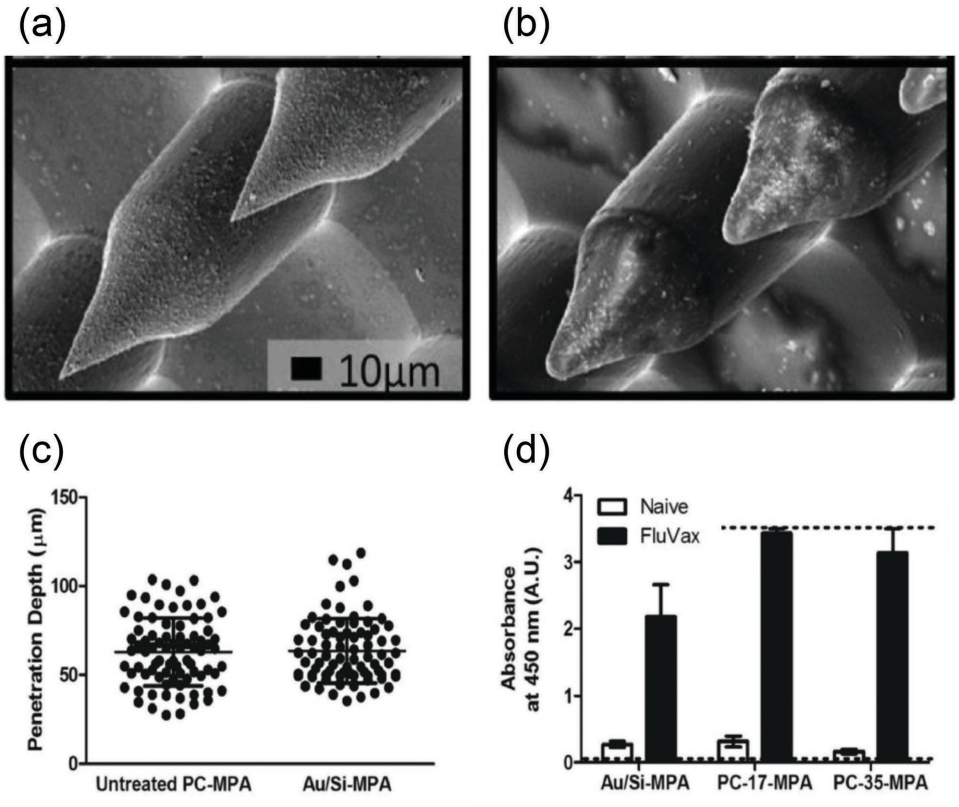

Figure 12. Polycarbonate MPAs for in vivo capture of circulating biomarkers. a,b) SEM images of PC-MPAs before and after application on the flank skin of live mice, respectively. c) Depth penetration measurements showing equivalent penetration depths for Au/Si- and untreated PC-MPAs. d) MPA-ELISA results showing direct capture of anti-Flu Vax-IgG from the flank skin of vaccinated mice in comparison to naïve controls. Reproduced with permission.[106] Copyright 2013, American Chemical Society.

aromatic substitution allowed the attachment of antifouling PEG coatings which immobilize the capture probe, namely FluVax. Gold-coated silicon-MPAs with FluVax probes immobilized over a PEG coating were used as control. Surface-modified PC-MPAs were successfully tested for the capture of circulating biomarkers (i.e., anti-FluVax-IgG) both in vitro and in vivo, that is in serum collected from FluVax-immunized mice and in the flank skin of FluVax-immunized mice, respectively. Mice were vaccinated with FluVax 2009 via intramuscular injection, and biomarker capture tests were carried out at day 14 after vaccination. After a 10 min application time, significant absorbance signals were achieved for PC-MPAs applied to vaccinated mice with respect to naïve mice used as a control (Figure 12d). Moreover, direct evaluation of both gold-coated silicon-MPAs and PC-MPAs showed comparable results for capturing anti-FluVax-IgG, with detection limits similar to Nunc Maxisorp ELISA surfaces used as a standard reference.

An alternative approach for the collection of biomarkers using microneedles for subsequent analysis by means of conventional analytical tools, such as microtubes and microplates, was recently proposed by Romanyuk et al.,[108] which reported in vivo extraction of ISF using hydrogel microneedle patches, which can swell in the presence of water (**Figure 13**). The fabrication of the hydrogel microneedle patches was carried out through a micromolding method, that is by casting a blend of 15% poly(methyl vinyl ether-*alt*-maleic acid) (PMVE/MA) and 7.5% PEG onto a PDMS micromold featuring a 10 × 10 array of conical cavities that were filled with the prepared solution under vacuum. After drying the microneedle patches for 24 h at room temperature, polymer cross-linking was obtained through a curing process at 80 °C at various times in the range 24–72 h. In their dry state, the resulting microneedles were 600 μm tall, 300 μm wide at the base and featured a tapered tip with a radius of curvature of ≈10 μm (Figure 13a). In vitro experiments were carried out to investigate volume swelling of hydrogel microneedles upon incubation in water for 24 h as a function of the hydrogel cross-linking time. An extended cross-linking time of 72 h yielded a 3-fold swelling in volume with low variability, whereas a less-extensive cross-linking time of 24 h yielded a more than 50-fold swelling in volume with high variability. In vivo extraction of ISF was given by manually applying the microneedle patches to rat skin for 1 h. As a negative control, patches with blunt-tipped microneedles were prepared with the same fabrication method, albeit using molds with blunt tips. Staining of the rat skin after patch removal confirmed that sharp-tipped microneedles were able to successfully penetrate the skin, whereas blunt-tipped control patches were not (Figure 13b). All patches were weighed before and after application to the skin, which indicated that microneedle patches extracted 0.84 ± 0.24 mg of ISF. A proof-of-concept method was then proposed with the aim to target analyte extraction from microneedle patches by integrating them into conventional microtubes and microplates (Figure 13c). Analyte-loaded patches

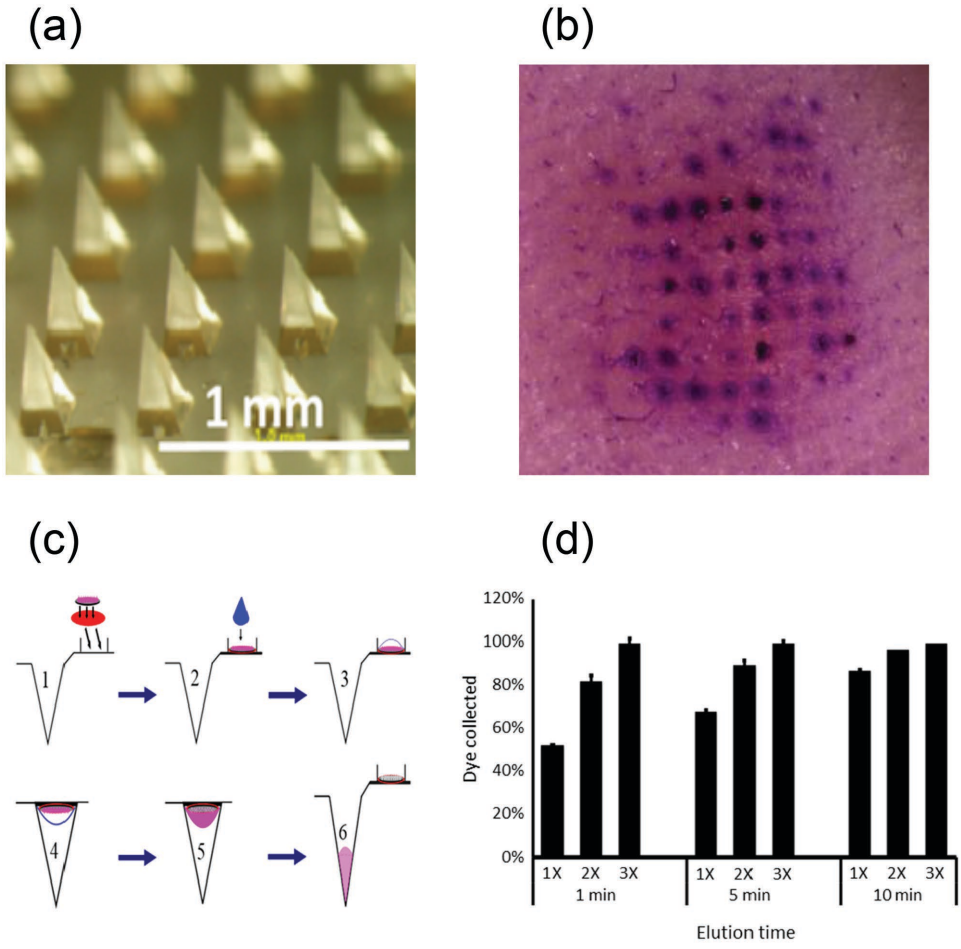

Figure 13. In vivo collection of analytes from swelling microneedle patches made of cross-linked hydrogel. a) A microneedle patch made of cross-linked hydrogel in its dry state. b) Rat skin after application of a microneedle patch and subsequent staining, proving effective microneedle skin penetration. c) Protocol for the collection of analytes from the microneedle patch by centrifugation. d) The percentage of analyte collected from microneedles into elution fluid after application of 100 µL of water for 1, 5, or 10 min and centrifugation at 300 *g*, which was carried out one (1×), two (2×), or three (3×) times. Reproduced with permission.[108] Copyright 2014, American Chemical Society.

being used to quantify the extraction of target analytes from microneedles were prepared using the dye sulforhodamine B as the model analyte. A double casting method was used to prepare microneedle patches with a controlled amount of dye. The first method employed microneedle patches affixed within the cap of microcentrifuge tubes. After dispensing a drop of water (100 µL) onto the microneedle patches and incubating the solution for 10 min to extract the model analyte, the cap was closed and the tube underwent centrifuge (20 s at 300 g) to collect the extracted analyte solution. The efficiency of the method was evaluated by varying incubation time (i.e., 1, 5, or 10 min) and number of process cycles (i.e., 1×, 2×, or 3×) (Figure 13d). Efficiency increased with both incubation time and number of cycles, with only 53% recovery of the model analyte for 1× cycle and 1 min incubation vs 100% recovery for 3× cycles, independent of incubation time.

3.3. Other Analytes

Investigation of physiological activities, such as the synthesis of proteins, regulation of body pH balance, and the release of neurotransmitters, is nowadays gaining more and more significance. Blood is full of proteins, mineral ions, hormones, and neurotransmitters that are commonly monitored in clinical blood tests. On the one hand, plasma proteins (such as transferrins, prothrombins, or globulins) and blood pH can be assessed to verify proper cellular activities[109,110] and acid-base homeostasis,[111] respectively. On the other hand, glutamate and electrolyte monitoring can provide valuable information on brain[112] and muscle[113] functions or on the body's hydration.[114] Scientists are now exploring alternative methods, such as microneedle-based approaches, to overcome the invasiveness of blood sampling methods making use of hypodermic needles routinely used in conventional test blood.

3.3.1. Single Analyte Detection

In 2007 Park et al.[115] reported about the use of a microneedle-based sensor for in vitro pH level detection as a first step towards either intracellular biochemical detection or analysis of localized bioenvironments in terms of the pH level and/or

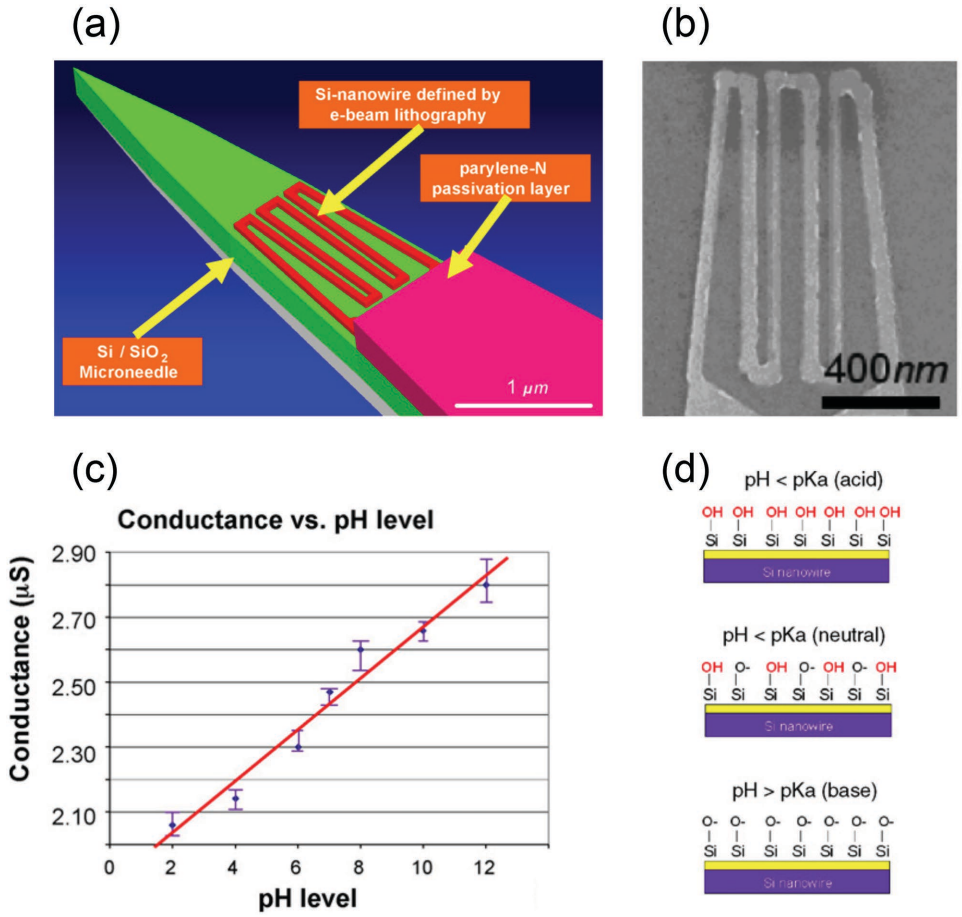

Figure 14. A microneedle sensor platform for intracellular biochemical detection. a) Sketch of the microneedle tip with an integrated serpentine silicon nanowire on it. b) SEM image of the silicon nanowire integrated on the microneedle tip. c) In vitro calibration curve of the nanowire sensor (conductance versus pH level) at different pH values from 2 to 12. d) Qualitative model for change of electrical conductance of the silicon nanowire as a function of different pH levels, as proposed by the authors. Reproduced with permission.[115] Copyright 2007, Elsevier.

enzyme activities (**Figure 14**). Intracellular pH regulation is critical for most cellular processes (such as cell volume regulation, cellular metabolism, cytoskeletal interactions, etc.); as a consequence, monitoring of this parameter is of chief importance in examining cell and organ functions.[116] Several techniques have been used to monitor pH, such as fluorescent spectroscopy, nuclear magnetic resonance (NMR), and pH sensitive microelectrodes.[117] Particularly, microelectrode-based measurements of intracellular pH involve the insertion of an electrode small enough so as not to damage the cell (i.e., with diameters ≤1 μm) through the plasma membrane and into the cytoplasm.[118] A sharp geometry of the sensing electrode was highly desired for both intracellular and extracellular biochemical sensing, in order to avoid interference with other individual cells, to achieve localized biochemical detection from particular position within/outside of the cells, and to cause minimal invasiveness to the cell membrane during intracellular detection tasks.

A two-step process was designed to fabricate a sharp microneedle, as follows: 1) a blunt needle structure was defined by photolithography and 2) further sharpened by focused-ion-beam (FIB) machining. In order to increase detection length in a small confined area and thus improve the sensitivity of the device, a silicon nanowire with a serpentine pattern (height of 50 nm, width of 100 nm, and length of 6 μm) was defined on top of the microneedle structure by electron-beam (e-beam) lithography followed by a reactive ion etching (RIE) process. The choice of silicon nanowire-based sensors was based on their numerous advantages, such as small quantity of analytes required for sensing, low interference with biochemical processes within cells, and the possibility to properly functionalize the sensor surface for multiplexed detection.[119,120] A sketch of the microneedle structure integrating the silicon nanowire is given in Figure 14a. Figure 14b shows an SEM image of the silicon nanowire. Parylene-N thin film passivation of the silicon nanowire between the electrical conduction path and surrounding environment (e.g., water-based, such as PBS) was performed to minimize the leakage current and electrical noise, and to avoid redox reactions at the metal surface. In vitro preliminary tests of the silicon nanowire-integrated microneedle sensor were carried out using various PBS solutions with pH values ranging from 2 to 12 (Figure 14c). The electric current flowing through the silicon nanowire sensor was continuously measured at a bias potential of 100 mV, which allowed for a

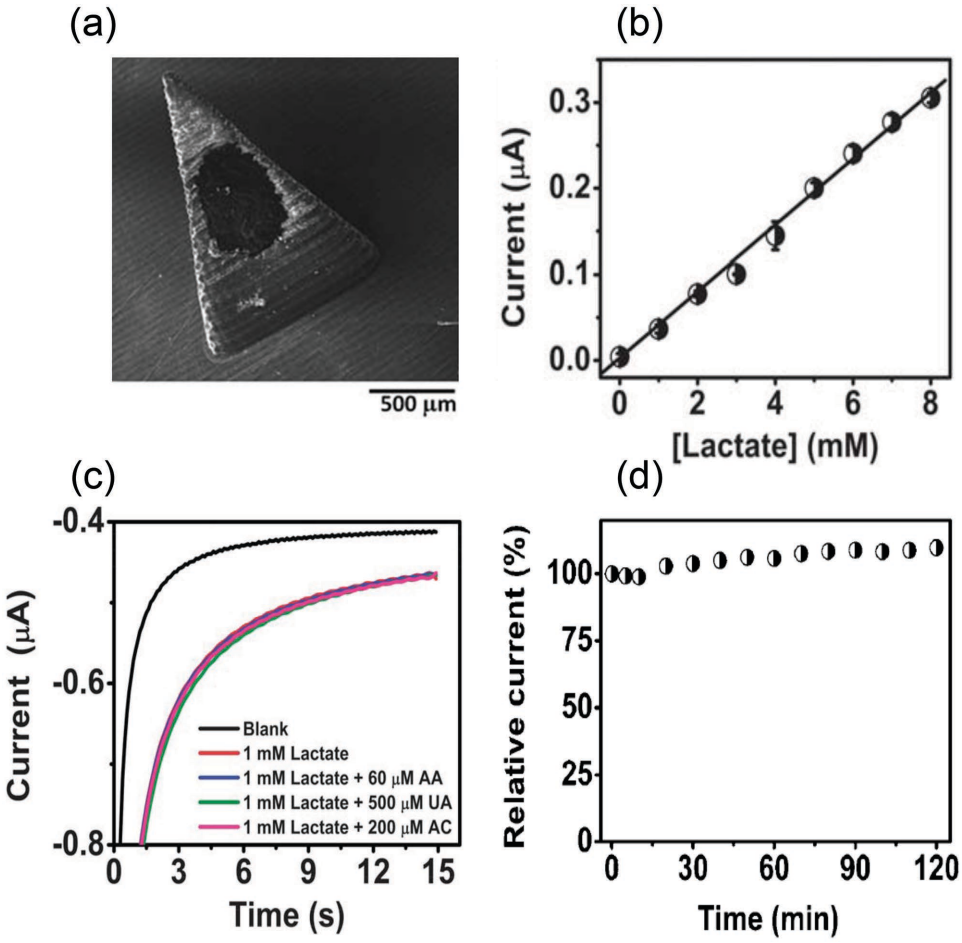

Figure 15. Microneedle carbon paste electrode arrays for in situ biosensing of lactate. a) SEM image of a rhodium-dispersed carbon paste packed microneedle. b) In vitro calibration curve of the microneedle electrode (current at 15 s versus concentration) for different lactate concentrations (0–8 mM). c) Interference study of the microneedle biosensor towards physiologically relevant electroactive compounds (AA, UA and AC). d) Stability of the electrochemical response of the microneedle biosensor for 2 mM lactate over a 2 h test. Reproduced with permission.[90] Copyright 2011, Royal Society of Chemistry.

reduction in redox reactions interfering with pH signal. The sensor showed a good linear relationship between pH level and electrical conductance of the nanowire with a sensitivity of 79.4 nS/pH, which was ascribed to modulation of the free-charge carriers into the nanowire upon surface charge field effect, this latter induced by changes in the proton ion (H^+) concentration around the nanowire itself (Figure 14d).

More recently, Windmiller et al.[90] reported the development and characterization of a microneedle-based carbon paste electrode (CPE) for in vitro lactate biosensing (**Figure 15**). CPEs have been widely used in electrochemical and electroanalytical measurements due to their several advantages, such as high degree of plasticity, low background current, and low fabrication cost.[121] Lactate ions ($CH_3CH(OH)COO^-$) result from the deprotonation of lactic acid from the carboxyl group, and are constantly produced from pyruvate via the enzyme lactate dehydrogenase (LDH) in a process of fermentation during normal metabolism and exercise. Lactate monitoring is important since high concentrations (>1–2 mM in human blood at rest) can reduce blood pH which, in turn, can cause damage to muscle tissues.[122] The microneedle array consisted of a 3 × 3 square array of hollow needles with 2 mm periodicity. The needles were pyramidal-shaped with a triangular base, edge length of 1250 µm, height of 1500 µm, and a vertical cylindrical bore of 425 µm in diameter on one of the faces of the pyramidal structure (Figure 15a). Fabrication of the microneedles was carried out by a standard UV rapid prototyping system that allowed for the selective polymerization of a photocurable material. The commercial E-shell 200 acrylate-based polymer[123] was used as the microneedle constituent material due to good mechanical properties (e.g., a Young's modulus of 2.4 GPa), high biocompatibility (i.e., Class-IIa) and low water absorption (i.e., 0.12%), which make this polymer suitable for biomedical applications (e.g., thin-walled hearing aid shells).[124] An enzyme-functionalized rhodium-dispersed CPE was prepared by homogenizing rhodium on carbon and lactate oxidase (LOx). Following the homogenization process, polyethylenimine (PEI) enzyme was added to the mixture to achieve the electrostatic entrapment of LOx within the matrix. The resulting LOx-dispersed metallized carbon paste was then extruded into the borehole of each microneedle of the array, thus achieving a rhodium-dispersed CPE microneedle array (Figure 15a). The biosensing

DOI: 10.1002/adhm.201500450

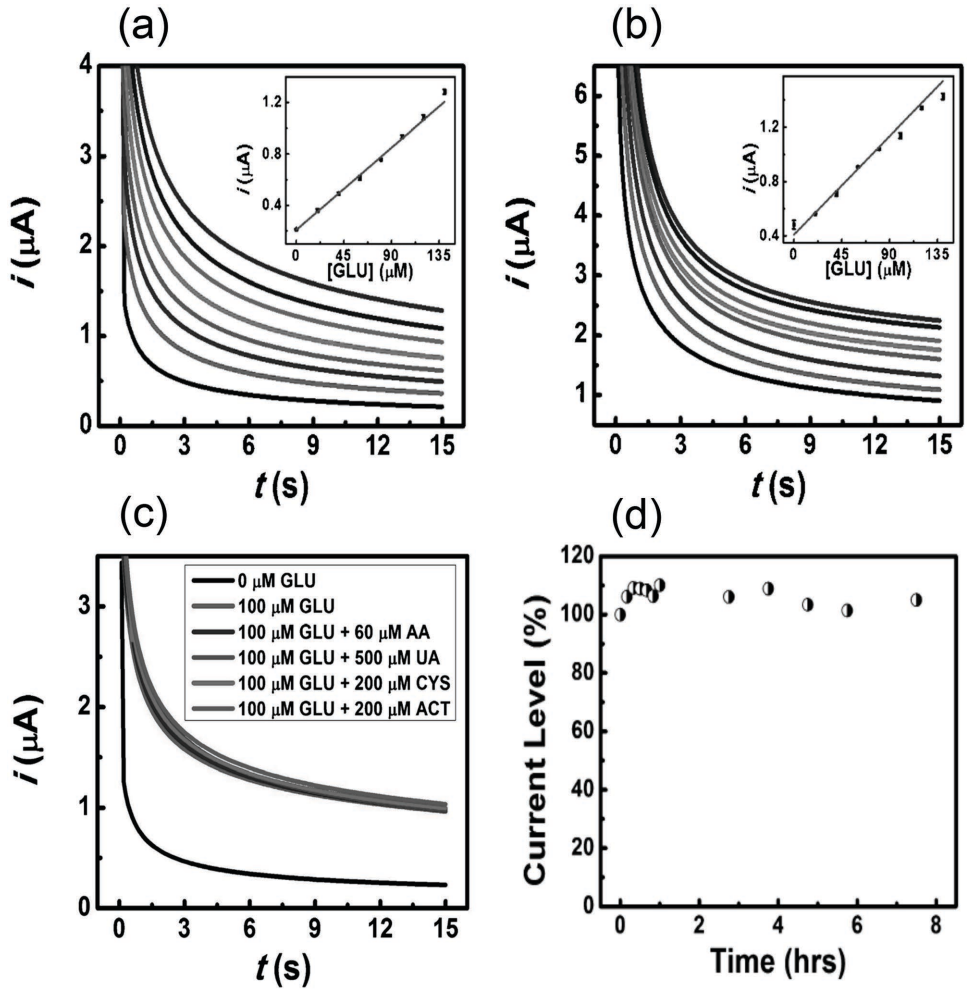

Figure 16. A bicomponent solid/hollow microneedle array biosensor for glutamate detection. a,b) Chronoamperograms recorded in vitro for increasing concentrations of glutamate (from 0 to 140 μM) in 0.1 M phosphate buffer and human serum, respectively. c) Selectivity of the microneedle biosensor in the presence of physiologically relevant electroactive compounds (AA, UA, CYS, and ACT). d) Time stability of the microneedle biosensor response to 100 μM glutamate over a period of 8 h. Reproduced with permission.[62] Copyright 2011, John Wiley and Sons.

performance of the LOx-rhodium-carbon paste microneedle array for lactate detection was investigated through in vitro chronoamperometric experiments at −0.15 V (vs Ag/AgCl) for increasing levels of lactate (from 0 to 8 mM in 1 mM increments). The calibration curve (obtained from chronoamperograms for current sampling at t = 15 s) showed high linearity (R^2 = 0.990) and low standard deviation (σ < 10 nA) over the entire physio-pathological range, with an estimated detection limit of 0.42 mM of lactate (S/N = 3) (Figure 15b). An interference study was then conducted to assess the functionality of the lactate biosensor in the presence of electroactive substances commonly found in transdermal fluids. Chronoamperometric tests were carried out at −0.15 V (vs Ag/AgCl) using 1 mM lactate in the presence of physiological levels of AA, UA, and ACT (Figure 15c). A negligible influence of the tested interferents on the lactate response was observed, with a maximum current deviation of only 1.5% from the 1 mM lactate level in correspondence of AC addition. The stability of the electrochemical response of the microneedle-based biosensor was finally investigated from repeated chronoamperograms for 2 mM lactate recorded over a period of 2 h (Figure 15d). The current, which was sampled every 10 min over the entire 2 h test period, highlighted high stability with only a slight increase of 9.7% over the whole measurement time, thus suggesting that the integrity of the microneedle biosensor was successfully retained.

In a similar work, Windmiller et al.[62] developed a bicomponent microneedle array biosensor for the electrochemical monitoring of glutamate (GLU) (**Figure 16**). GLU is an amino acid serving as a neurotransmitter at many excitatory synapses in the mammalian central nervous system (CNS). GLU plays an important role in many brain functions being implicated in several pathologic conditions, such as epilepsy, Alzheimer's disease, etc. Normal human-blood-GLU concentration is around 10 μM[125] and monitoring of GLU levels can provide valuable information on the patient's CNS conditions. Recently, clinical studies revealed that blood GLU levels correlate well with GLU levels found in the cerebral spinal fluid,[126] which motivated the use of microneedle-based devices for GLU sensing as a minimally invasive approach alternative to standard painful extraction of such a hard-to-access bodily fluid.

The bicomponent microneedle array consisted of solid and hollow microneedles integrated together into a single biosensor array device containing multiple microcavities, as described in Section 3.1. However, a different PPD growth protocol based on a three-step process was used to entrap glutamate oxidase (GLUOx) enzyme within the microcavities resulting from the integration of solid and hollow microneedles. An initial electrochemical characterization of the bicomponent microneedle array was carried out to optimize the detection potential (0.40 V vs Ag/AgCl) so as to minimize the potential oxidation of interferents in real samples. The sensitivity of the microneedle-based device was then evaluated both in buffer matrix and human serum through chronoamperometry. In particular, chronoamperometric experiments were performed at increasing levels of GLU over the entire pathophysiological range (0–140 μM in 20 μM increments) both in 0.1 M PBS solution and undiluted human serum samples (Figure 16a,b). For PBS solution, the calibration curve obtained at $t = 15$ s showed a linear behavior ($R^2 = 0.995$) over the whole tested range, with high sensitivity ($S = 7.129$ nA μM^{-1}) and low standard deviation (RSD = 3.51%, $n = 3$). An LOD of 3 μM was extrapolated based on the signal-to-noise characteristics of the experimental data (S/N = 3), which was well–below standard physiological levels, thus revealing the ability of the microneedle sensor to detect physiological levels of GLU. As for PBS, a linear calibration curve was obtained in undiluted human serum over the whole tested range ($R^2 = 0.992$), with high sensitivity ($S = 8.077$ nA μM^{-1}), low standard deviation (RSD = 6.53%), and an LOD of 21 μM (S/N = 3). The selectivity of the system was further demonstrated in the presence of physiological levels of common electroactive interferents (60 μM AA, 500 μM UA, 200 μM CYS, and 200 μM AC), which resulted in negligible deviations (average values in the range of 0.31%–6.37%) from the 100 μM GLU current response (Figure 16c). The stability of the bicomponent microneedle response to GLU was finally verified over a period of 8 h using a 100 μM GLU solution (Figure 16d). The time-course profile indicated a highly stable current response retaining 105% of the original signal level after the whole time period, thus highlighting the possibility to use the microneedle sensor as a patch-type on-body biosensors toward a continuous and in vivo quantification of GLU in a minimally invasive manner.

Esfandyarpour et al.[127] proposed a microneedle biosensor as a real time, label-free, and localized device for detection of target proteins, which are of great interest in several health-related fields such as medicine, biotechnology, genetics and others. Two different microneedle arrays (namely horizontal and vertical) were designed, although the proof of concept of such a novel microneedle biosensor was only given for the horizontal design. The horizontal microneedles were composed of a three thin-film structure anchored to a silicon substrate with a free-standing tip; this latter protruded over a PDMS microchannel bonded to the silicon substrate integrating the microneedle array. The microneedle tip consisted of two conductive layers made of doped polysilicon films acting as top and bottom electrodes, with a third insulator layer made of a SiO_2 film in between. Two further layers consisting of SiO_2 films above and below the microneedle structure were used to insulate the bottom polysilicon electrode from the silicon substrate and to act as a protective layer to avoid exposure of the top polysilicon electrode to tested solutions, respectively. The fabrication process of the horizontal microneedle biosensor fully relied on silicon technology steps, namely thermal oxidation, deposition processes, doping, and etching phases. For one of the tested microneedle biosensors, the thickness of each electrode was 100 nm, the middle oxide layer thickness was 20–30 nm, the top protective oxide layer thickness was 200 nm and the bottom oxide layer thickness was 250 nm. The width of the microneedle tip was 5 μm. The proof of concept for protein detection with the microneedle biosensor was given by in vitro testing of the device's ability to detect binding of biotinylated BSA (which acted as the receptor protein) and streptavidin (which acted as the target analyte) in real time. A PBS solution was injected into the microchannel and the impedance between the two electrodes was measured and used as the baseline impedance to which all changes were referred. Biotinylated BSA molecules suspended in PBS (100 μg mL^{-1}) were subsequently injected in the microchannel. After protein physical adsorption to the oxide surface of the needle reached its steady-state condition, streptavidin (10 μg mL^{-1} in PBS) was in turn injected into the channel and its binding to the surface-attached biotinylated BSA molecules was monitored. As a control, PBS was injected into the microchannel and the impedance was measured to confirm that changes of impedance were due to the attachment of molecules to the sensor area. The typical binding curve (i.e., impedance variation) over time showed a ≈5% change in impedance after the binding of streptavidin molecules to the biotinylated BSA. Finally, two control experiments (namely, positive and negative control tests) were successfully carried out to assess the specific streptavidin binding to the biotinylated BSA molecules by making use of fluorescently labeled streptavidin molecules.

Recently, Miller et al.[128] reported the first example of an ion selective microneedle-based transdermal sensor for on-chip potentiometric determination of potassium ions (K^+) (**Figure 17**). Among the myriad of analytical targets of the human body (e.g., proteins, nucleic acids, metabolites, etc.), electrolytes (i.e., mineral substances in human blood) play an important role in healthcare assessment since they regulate nerve and muscle functions, the body's hydration, blood pH, and other important processes.[129] The main electrolytes in the body are potassium and sodium (other electrolytes are chloride and bicarbonate), and electrolyte testing is usually carried out as part of routine blood tests. In their work, Miller et al. integrated a polymer hollow microneedle with a microfluidic chip to extract fluid through a channel and to determine physiologically relevant concentrations of K^+. E-shell 300 was used as the biocompatible material to fabricate the microneedle (width of 440 μm, height of 1450 μm, and triangular bore of 165 μm), which was achieved through a two-photon polymerization technique onto a removable substrate that could fit within a pre-defined recess on the microfluidic chip[124] (Figure 17a). The microfluidic chip consisted of a poly(methyl methacrylate) (PMMA) substrate featuring a fluidic microchannel (width of 870 μm) that connected, in turn, the microneedle with a three-electrode system integrated in the microchannel itself (Figure 17b). Two different working electrodes, namely pyrolyzed carbon (pC) and porous graphene (pG), were fabricated and tested as potential novel solid-state ion selective electrodes (ISE). While both

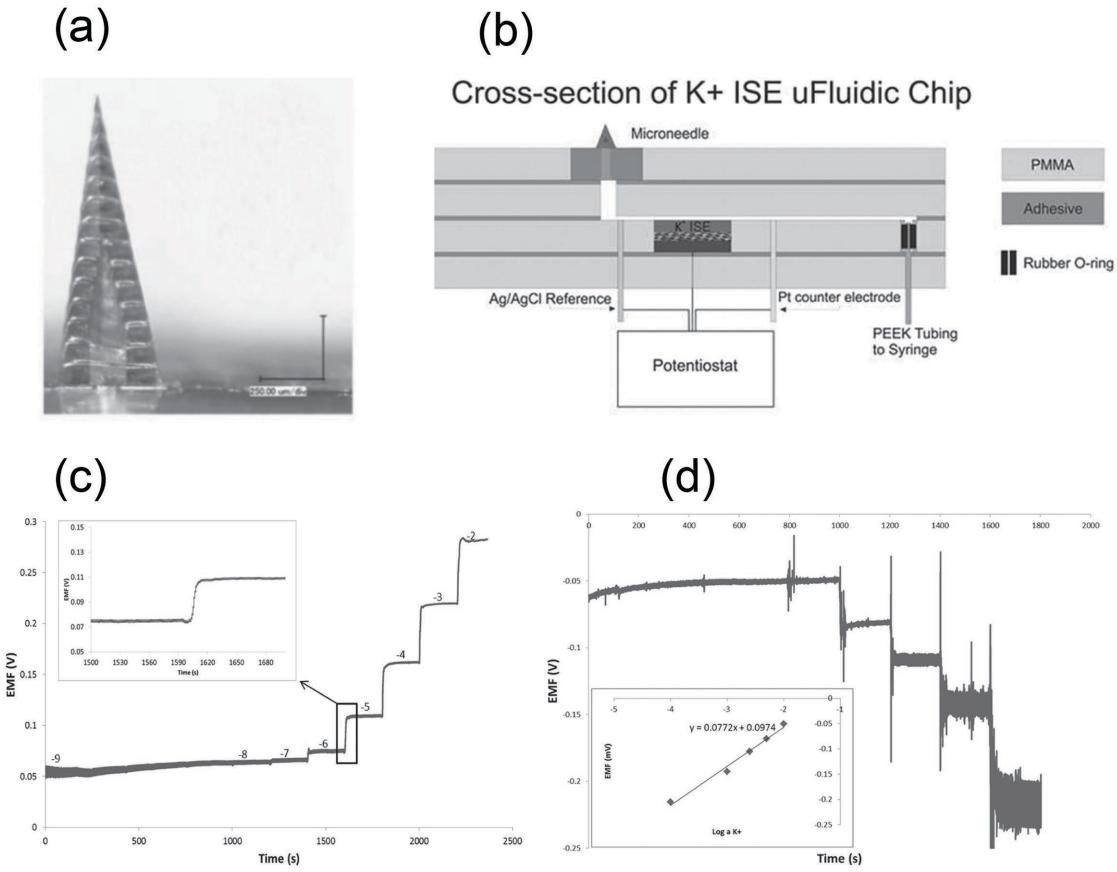

Figure 17. An ion selective microneedle-based transdermal sensor for potentiometric K^+ detection. a) Optical image of a hollow polymer microneedle made using a two-photon lithography process. b) Sketch of a cross-section of the K+ ISE microfluidic chip showing the microneedle connected to a three-electrode sensor. c) Electromotor force measurements of the porous carbon K^+ selective electrode for increasing concentrations of potassium. d) On-chip calibration for varying physiologically relevant KCl concentrations. Reproduced with permission.[128] Copyright 2013, John Wiley and Sons.

were capable of lowering the membrane resistance of the ISE's when compared to glassy carbon electrodes, the pC electrodes showed better electrochemical performance. pC/K^+ ISE's exhibited a detection range from 10^{-5} to 10^{-2} M with a near Nernstian slope of 57.9 mV per decade, a rapid stabilization (≈20 s), and no significant response to interfering Na^+ (Figure 17c). The pC/K^+ ISE's were integrated into the microneedle sensor due to their higher electrochemical performance and stability over pG using an Ag/AgCl wire and a Pt wire as reference, and counter electrodes, respectively. For on-chip measurements, KCl solutions at different K^+ concentrations were flowed through the microneedle into the fluidic channel via a syringe and allowed to stabilize for 200 s, then measured downstream at the pC/K^+ ISE (Figure 17d). A linear response was observed for the tested values with an ideal Nernstian response, after subtracting the influence of ionic dissociation due to the Ag/AgCl wire from the measured values. The on chip response of the pC/K^+ ISE after fluidic introduction of K^+ through the microneedle was sensitive to physiological potassium levels, indicating the chip was capable of rapidly and selectively measuring clinically relevant samples corresponding to normal and abnormal concentrations.

In 2014, Vazquez et al.[130] proposed a microneedle sensor based on the integration of microscopic gel-liquid interfaces within a hollow silicon microneedle array for in situ voltammetric drug detection. Micro-interfaces between two immiscible electrolyte solutions (μITIES) have been recently and successfully proposed for the electrochemical detection of several species (e.g., amino acids, neurotransmitters, drugs, etc.).[131] Electrochemistry at the μITIES is based on the transfer of ions across a polarized liquid-gel interface upon application of a voltage difference, which leads to an increment of current through the interface.[132] The hollow silicon microneedle arrays (height of 300 μm, spatial period of 1 mm, bore-hole diameter between 55 and 62 μm) were fabricated using a combination of potassium hydroxide (KOH) wet-etching and Bosch dry-etching techniques. The creation of μITIES at the microneedles was performed by filling their bores with an organogel made of 1,6-dichlorohexane (1,6-DCH) and low molecular weight polyvinylchloride (PVC) in a 10:1 volume to weight ratio. Two different in vitro electrochemical characterizations were carried out, namely cyclic voltammetry (CV) and differential pulse stripping voltammetry (DPSV), to investigate the electrochemical response of the hollow microneedle system and to demonstrate successful drug detection, respectively. As to the former, CV curves (scan rate of 35 mV s^{-1}) of 160 μM of the model analyte tetraethyl ammonium cation (TEA^+) revealed that an increment of the current flowing through the electrochemical

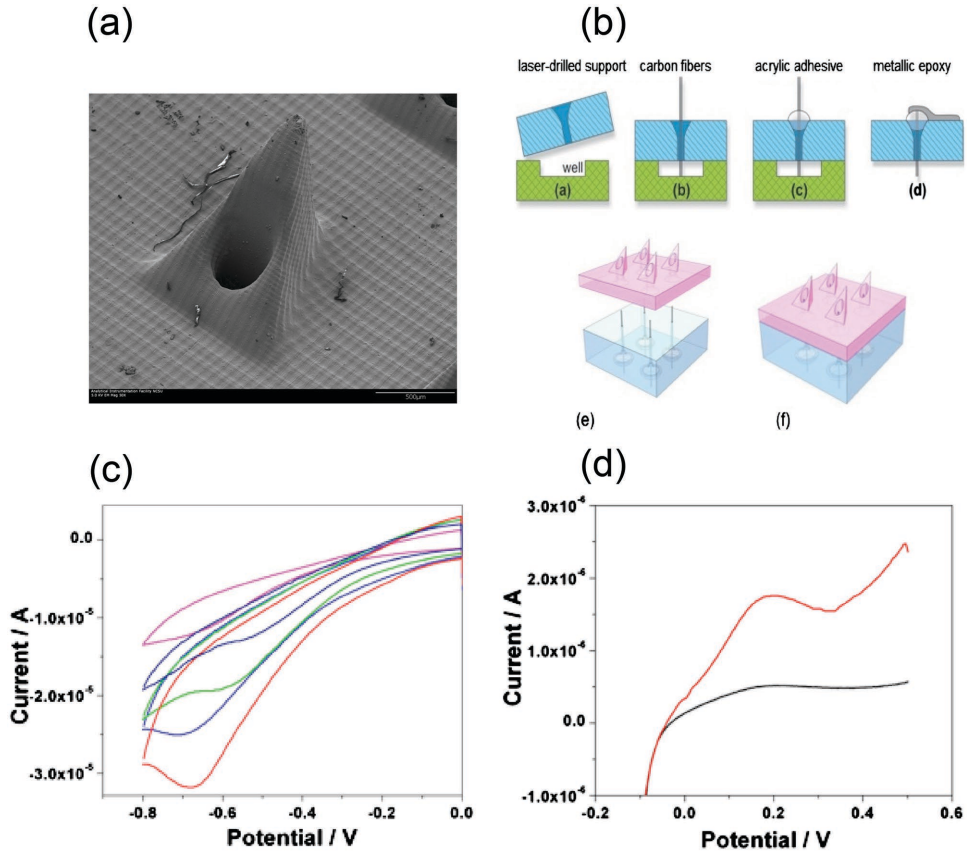

Figure 18. Integrated carbon fiber electrodes within hollow polymer microneedles for electrochemical sensing of H_2O_2 and AA. a) SEM image of a single hollow microneedle after the incorporation of carbon fiber electrodes. b) Schematic of the main fabrication steps for the assembly of the microneedle sensor. c) In vitro cyclic voltammetric scans for different concentrations (0–500 μM) of H_2O_2. d) Linear sweep voltammograms in the presence of AA 0 mM (black curve) and 1 mM (red curve) in 100 mM phosphate buffer. Reproduced with permission.[135] Copyright 2011, AIP Publishing LLC.

cell was visible when TEA^+ diffused from the aqueous phase toward the organogel; conversely, a peak current was achieved on the reverse scan, indicating a diffusion-controlled process when TEA^+ moved back to the aqueous phase. Propranolol was then used as a model drug. Propranolol is a sympatholytic non-selective beta-blocker and is used for the treatment of several pathological conditions, such as hypertension, angina pectoris, tachycardia, etc.[133] Heart rate and blood pressure correlate with propranolol levels in plasma; therefore, its measurements can be used to tailor drug dosage or to monitor patient response after treatment.[134] CV curves (scan rate of 8 mV s^{-1}) of 100 μM propranolol at the liquid-gel interface of the microneedle array showed the same trend as CV curves obtained with TEA^+, with hemispherical diffusion during the forward scan and linear diffusion during the reverse scan. Further DPSV analysis was used to find out the sensitivity and detection limit of the microneedle sensor. After determining the optimum preconcentration time $t = 240$ s to maximize the current peak, DPSVs for increasing concentrations (from 0.03 to 1 μM) of propranolol in aqueous solution were recorded, from which the corresponding calibration curve was assessed by monitoring the stripping current peak. A linear increment ($R^2 = 0.994$) of the stripping peak was obtained for propranolol concentrations in the range 50–200 nM, with a sensitivity of 43 nA μM^{-1} and a LOD of 50 nM. Lower concentrations showed a behavior typical of spherical diffusion, whereas higher concentrations caused the stripping peak current to saturate.

3.3.2. Multi Analyte Detection

Previously reported approaches have focused on the design of microneedle-based sensors for transdermal sensing of single analytes. However, a number of recent studies have also paid specific attention to the development of microneedle-based sensors for transdermal detection of multiple analytes within the same platform, so as to perform multiplexed sensing. Such an approach has been inspired by the arrayed nature of the microneedles themselves, which allows in principle to use each (or a cluster of) microneedle(s) in the array to detect a particular target analyte. In this way, multiplexing of the sensed analytes has been enabled over the whole array of microneedles, thus increasing health-targeted biological information collected simultaneously.

Dating back to 2011, Miller et al.[135] reported the fabrication and characterization of carbon fiber electrodes integrated into hollow microneedles for simultaneous in vitro electrochemical sensing of two clinically relevant molecules, namely hydrogen peroxide (H_2O_2) and AA (**Figure 18**). H_2O_2 is a reactive oxygen species largely detected by many enzyme-based

electrochemical sensors, such as glucose or glutamate biosensors.[136] AA is an analyte that has recently been employed as an indicator of oxidative stress experienced by cells.[137] Tetrahedral-shaped hollow microneedle arrays were fabricated using E-shell 200 polymer as the constituent material, by digital micromirror device-based stereolithography, this being a technique that has been widely used to produce scaphoid and lunate bone prostheses[138] or tissue engineered scaffolds.[139] The microneedles exhibited heights of 1030 µm, triangular bases with side lengths of 1120 µm, and bore diameters of 375 µm (Figure 18a). The needles were arranged into a 2 × 2 square array with 2 mm spacing. Penetration tests performed with full-thickness cadaveric porcine skin successfully proved microneedle insertion in skin without damage to the needle structure. Carbon fiber electrodes were then incorporated within the bores of each hollow microneedle through a manual precise alignment process. Afterwards, the fibers were secured in place with acrylic adhesive on a PMMA substrate provided with a square pattern of holes with widths of 45 µm and spacings of 2 mm, thus replicating the needle array pattern. A sketch of the fabrication process is given in Figure 18b. Carbon fibers were chosen mainly due to their good biocompatibility.[140,141] SEM analysis of the hollow microneedles after the incorporation of carbon fibers showed that the alignment process yielded a good positioning of the electrodes, which did not extend beyond the tip of the microneedle bore. Palladium deposition and aminophenol (o-AP) group modification were carried out on the carbon fibers before their insertion into the microneedle device so as to enable the detection of H_2O_2 and AA, respectively. An electrochemical characterization of the chemically modified carbon fiber needles was then performed in the presence of both H_2O_2 and AA. A preliminary electrochemical response of the carbon fibers within the hollow microneedle device was carried out using a 5 mM $Fe(CN)_6^{3-/4-}$/1 M KCl solution. The cyclic voltammetric scan (scan rate of 100 mV s^{-1}) of 5 mM ferricyanide in 1 M KCl vs Ag/AgCl and Pt reference and counter electrodes, respectively, showed well defined oxidation/reduction peaks, indicating interaction between the carbon fiber electrodes and the test solution as a result of permeation of the solution into the microneedle bore. Palladium-catalyzed oxidation of H_2O_2 on the carbon fibers within the hollow microneedle devices was then investigated. Palladium was deposited onto the carbon fibers by applying a potential of –0.8 V for 120 s in 1 mM Pd/0.5 M HCl prior to insertion into the microneedle device. Cyclic voltammetric scans (scan rate of 100 mV s^{-1}) of 0 to 500 µM H_2O_2 vs Ag/AgCl and Pt reference and counter electrodes, respectively, showed an increase in reductive currents after additions of H_2O_2, exhibiting a linear range of 100–500 µM and a detection limit of about 15 µM (based on the response of 50 µM H_2O_2, S/N = 3) (Figure 18c). Finally, the ability of o-AP modified carbon fibers within the hollow microneedle device for the detection of AA was considered. Modification of the carbon fibers was carried out following in situ diazotination and electrografting of the corresponding diazonium salt. Linear sweep voltammograms (scan rate of 100 mV s^{-1}) of 100 mM phosphate buffer (blank solution) and 1 mM AA in 100 mM phosphate buffer (pH = 7) vs Ag/AgCl and Pt reference and counter electrodes, respectively, indicated that the carbon fibers within the hollow microneedle device were able to detect the ascorbate analyte with the low potential oxidation of AA at 195 mV (Figure 18d).

One year later, the same group[142,143] proposed the use of microneedle-based biosensors for in vitro simultaneous detection of three different physiologically relevant analytes using the same polymeric hollow microneedle array described by Miller et al.[135] However, the borehole of such needles was then selectively filled with different carbon paste electrodes properly modified to detect pH, glucose and lactate. The pH sensitive electrodes were obtained by chemically depositing 20 µL of a Fast Blue RR diazonium salt (4-benzoylamino-2, 5-dimethoxybenzenediazonium chloride hemi (zinc chloride) salt) solution on carbon paste. The glucose sensitive electrodes were gained by mixing GOx, PEI, and rhodium on carbon powder. Finally, the lactate sensitive electrodes were prepared using rhodium-modified carbon paste containing LOx.[90] Calibration of chemically modified carbon paste electrodes for detecting alterations in pH was performed in 0.1 M phosphate buffer over a 5.0–8.0 pH range at intervals of 0.5 pH units. Cyclic voltammetric scans were performed from –0.7 V to 0.8 V at 100 mV s^{-1} against an external Ag/AgCl reference and Pt counter electrodes. The pH response was measured by evaluating the shift of the anodic peak potential position of the quinone moiety on the immobilized Fast Blue RR salt. The calibration curve of the modified carbon paste electrodes for the tested pH range showed a negative shift of the oxidative peak potential with increasing buffer acidity, and a highly linear behavior (R^2 = 0.99) over the entire range of tested pH values. The response of carbon paste electrodes modified with GOx (for glucose detection) and LOx (for lactate detection) was then evaluated in 0.1 M PBS for different pH values (i.e., 5.0, 6.0, 7.0, and 7.5), against an external Ag/AgCl reference and Pt counter electrodes. The chronoamperometric detection potentials for glucose (–0.05 V) and lactate (–0.15 V) sensing were selected to catalytically reduce enzymatically produced peroxide while minimizing responses of common interfering electroactive species, such as AA, UA, and ACT. The calibration curves were linear for both the tested analytes and pH values over physiologically relevant concentration ranges (i.e., 0–12 mM for glucose and 2–12 mM for lactate). Multiplexed real time detection was eventually investigated to verify the capability of the microneedle-based biosensor platform to simultaneously detect different analytes with high accuracy and minimal cross-talk. To this end, mixtures containing glucose and lactate at a fixed pH value were used. The response of the lactate-sensitive microneedles of the array was evaluated by subsequently adding 4 mM glucose and 4 mM lactate to the buffer solution. The addition of glucose did not cause any significant response from the LOx-modified microneedles, whereas the addition of lactate produced a current response of ≈38 nA, in agreement with former calibration. The response of the glucose-sensitive microneedles of the array was considered through the addition of 4 mM of lactate followed by 4 mM of glucose to the buffer solution. The addition of lactate had no effect on the GOx-modified microneedles, whereas the addition of glucose produced an increase in current response of ≈10 nA, in agreement with the former calibration. The pH value was simultaneously confirmed from the response of the Fast Blue RR-modified microneedles of the array, thus concluding that each of the microneedle-electrodes in the array was

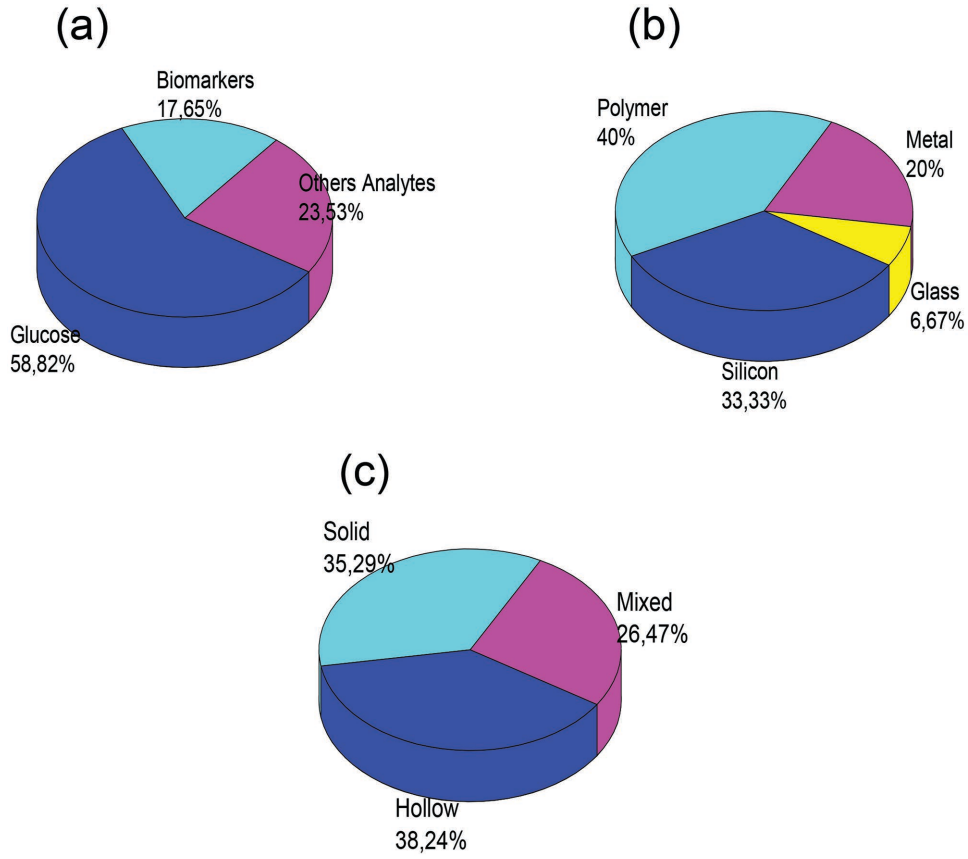

Figure 19. Pie charts classifying microneedle-based transdermal (bio)sensors on the basis of a) analyte, b) needle material and c) needle architecture.

capable of performing analyte-specific detection in a complex environment.

4. Current Picture and Future Direction

As pointed out in the previous sections, in the last decade a novel and exciting trend focused on the application of microneedles for analyte detection at the transdermal level has clearly delineated. Such a new course directly evolves from and perfectly complements the former trend on the use of microneedles for drug delivery, which has now reached its technological and clinical maturity. In spite of the relatively short time span on biosensing via microneedles, about 15 years from the first report, tremendous progress has been made, which has allowed moving on from the first attempts of using microneedles for in vitro glucose monitoring to commercial microneedle-based glucometers available on the market today.[144] For instance, ArKal Medical Inc.[37,82] has recently commercialized a microneedle-based CGM system that exploits a standard GOx chemistry formulation to be used without extraction of ISF. In detail, an array of tapered hollow silicon microneedles is used to enable passive diffusion of glucose from ISF beneath the outer layer of skin to a biosensor external to the microneedle chip. The CGM system has shown good in vivo performance on diabetic subjects with about 75% Region A in the Clarke Error Grid and a MARD of 15%.

Glucose monitoring has shown to be the major target of microneedle transdermal biosensors so far, driven by the increasing number of deaths caused by diabetes (and related complications) all over the world, which is today the 7th most common cause of death. To date, about 60% of the papers published on the use of microneedles for biosensing deals with glucose monitoring (**Figure 19**a). The remaining 40% mostly concerns papers published in the last five years and is equally split between the detection of biomarkers and other analytes (e.g., proteins, acids, ions, drugs, etc.). On the one hand, a great effort has been paid in the last few years to in situ detection of biomarkers for the early diagnosis of viruses. Although tests on humans have not been carried out as yet, in vivo experiments on animal models have been successfully performed and demonstrate the high potential of microneedles for such an application. On the other hand, a number of in vitro studies have recently been published on the use of microneedle-based sensors for in situ monitoring of the concentration of a number of analytes, such as proteins, ions, drugs, etc., of clinical interest. Thus the possibility to widely extend the application of microneedles within the field of clinical analysis is envisaged.

Besides analyte broadening, the use of microneedles for biosensing also encompasses a variety of architectures (i.e., hollow, solid, and combinations of them) and materials (i.e., metal, silicon, polymers, and combinations of them) that have been experienced over the years (Figure 19b,c).

Adv. Healthcare Mater. **2015**,
DOI: 10.1002/adhm.201500450

As for the needle architectures, hollow microneedles made of either metal or silicon-silicon dioxide have mostly been employed for biological fluid extraction, either blood or ISF, and ex situ glucose detection, using both in-chip biosensors and off-chip instrumentation. On the other hand, either solid microneedles coated with peculiar materials (e.g., Pt, PEDOT, PEG, CNTs, etc.) or hollow microneedles filled with functional materials (e.g., carbon paste, carbon fiber, microgel) have recently been used for in situ monitoring of glucose, biomarkers and other analytes. The in situ approach offers the advantage of detecting a passive accumulation of analytes on the functional material in contact with the needles, once these needles are inserted in the skin, without the need of external pumps for biological fluid extraction. Self-powered hollow microneedles have also recently been reported for ISF collection by exploiting only capillarity, again without the need of external pumps.

As for the needle materials, about 80% of papers on microneedles for biosensing reports on the use of needles exploiting either polymer (40%) or silicon-silicon dioxide (40%) as constituent materials, with the use of polymeric materials significantly increased over the last few years due to the facile and rapid fabrication. The remaining 20% of the studies makes use of metallic microneedles, which are still in use, though less and less over the years due to their more complex and expensive fabrication.

The analysis of state-of-the-art developments concerning the use of microneedles for biosensing applications highlights noteworthy results that have been achieved by microneedle-based devices for transdermal detection of a number of analytes of clinical interest. Nonetheless, it is also clear that a few key issues have been overlooked at this initial stage of the research, which need to be addressed in future towards real PoC applications. This aspect becomes apparent if the main features that would be required for an ideal microneedle-based device for transdermal PoC applications are delineated, which from our personal point of view are: 1) efficient interaction with skin, with a) effective skin penetration of needles and b) reliable needle-tissue interlocking, to allow the needles to reliably interact with skin and collect analytes from tissues; 2) effective on-chip biosensing, with a) efficient analyte collection on the needle-chip and b) excellent on-chip analytical sensing performance (i.e., in terms of accuracy, selectivity, LOD, sensitivity and reproducibility), to allow successful gathering of analytes of clinical interest through the needles and enable direct quantification of analytes at the chip level; 3) integrated on-chip sensors, with a) an on-chip transduction device and b) the availability of a miniaturized readout system, to allow transduction of the analyte signal at chip level without the need of bulky external instrumentation that would limit the biochip portability.

By taking into account these six chief parameters, a figure-of-merit can be depicted for each of the three classes of microneedle-based transdermal sensors that were identified in this review, namely for glucose sensing, biomarker detection, and measurement of other analytes. **Figure 20** shows radar plots aimed at providing a figure-of-merit for each class of microneedle-based transdermal sensors in terms of the above-mentioned main features rated over the range 1–5 (1: research at its early stage, 5: research at preindustrial stage). Microneedles for transdermal glucose sensing represent the most advanced corner of research in this field, being that most of the issues dealing with ideal features have already been successfully addressed, especially in terms of skin penetration, on-chip analyte collection, analytical performance, and on-chip sensor integration. Biomarker detection at the transdermal level using microneedles is also rapidly emerging and a few key issues have already been effectively addressed, such as skin penetration, on-chip analyte collection, and analytical performance. Finally, detection of other analytes of clinical interest using microneedles operating at the transdermal level is still in its infancy, although some preliminary works have been carried out in the last years with encouraging results. It is apparent that only a few analytes present either in blood or in ISF among the plethora of which are of clinical interest have been taken into account using microneedles so far, leaving a large gap for further research in this field. In fact, regardless of needle architecture, it can be easily envisioned that the sensing of further analytes of clinical interest at the transdermal level will drive microneedle-based biosensor research in the short-term future.

Independent from the sensed analyte, it is evident from Figure 20 that at least two key issues have been so far overlooked and need to be addressed toward real applications, namely the effective interlocking of needles with skin and the availability of a miniaturized system for driving/reading out the sensor.

The capability of needles to interlock with tissues is of primary importance to guarantee the reliability of the interaction process of microneedles with the biological system under investigation and, in turn, the reproducibility of analyses carried out through them, regardless of whether these analyses are performed in situ or ex situ. An unreliable interlocking of microneedles with skin would lead to poor reproducibility of the analyte collection process on/through the microneedles and, in turn, to poor accuracy of the measurement process of a specific analyte. Such an issue is even more important for microneedle-based devices aiming at continuous operation over time, with respect to one-shot operation devices. Recently, Yang et al. reported an interesting study focusing on the in situ mechanical interlocking of microneedles with tissues after their insertion into porcine skin.[145] A polymeric coating (namely, polystyrene-*block*-poly(acrylic acid) (PS-*b*-PAA) block copolymer), which swelled on contact with water after insertion of the needles in skin, was used to cover solid needles. In such a way, the interlocking of needles expressed in terms of tissue adhesion strength within the skin was significantly improved (0.93 ± 0.23 N cm^{-2}) with respect to both flat polymeric films used as controls (0.22 ± 0.09 N cm^{-2}) and commonly used staples (0.28 ± 0.11 N cm^{-2}). Accordingly, achieving significant adhesion to soft tissues while minimizing tissue damages poses considerable challenges that need to be effectively tackled in the near future toward real-world applications of microneedles for transdermal biosensing.

The readiness of miniaturized driving/readout system to be coupled with the sensor is related to the possibility of realizing PoC hand-held devices, which would be able to perform analyses in real-time where and when necessary. In fact, if the optimization of both microneedle architecture and sensor performance has been thoroughly investigated for different analytes,

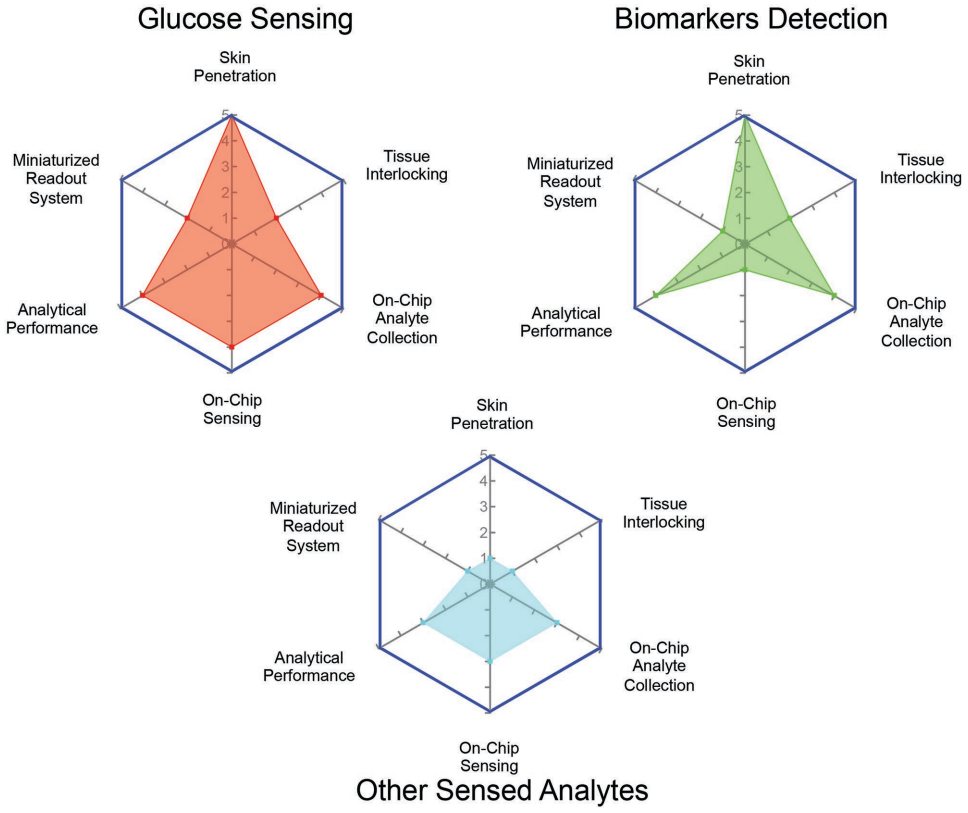

Figure 20. Radar plots depicting a figure-of-merit for each of the three classes of microneedle-based transdermal (bio)sensor detailed in this review. For each analyte (or class of microneedle) addressed, the plot instantly shows how far/close the specific class of microneedle-based (bio)sensors is from/to an ideal microneedle-based device for transdermal PoC applications (blue line), which was defined on the basis of 6 chief parameters identified as of major importance by the authors. An arbitrary unit scale with values ranging from 1 to 5 was used to rate the 6 parameters, where 1 indicates research at an early stage and 5 indicates research at a pre-industrial stage.

the miniaturization of the driving/readout system of the on-chip sensor has been overlooked so far. As such, most microneedle devices based on both electronic and photonic approaches have been characterized using lab-scale equipment, which hinders the real potential of microneedle-based devices for point-of-need measurements. A miniaturized driving/readout system, possibly integrated on the microneedle chip itself and making use of radio frequency identification data (RFID) circuits for on-demand biasing of the sensor and wireless transmission of sensor data to mobile phones for an easy-to-access storage and management of the data, represents a possible long-term period of development for microneedle transdermal biosensors.

5. Conclusions

In the last decade an increased research effort has been directed towards the use of microneedles for transdermal (bio)sensing of a number of analytes of clinical interest, such as glucose, biomarkers, and many others. This new trend has germinated naturally from former efforts on the use of microneedles for drug delivery, perfectly complementing it. The challenge is the realization of pain-free and easy-to-use miniaturized biochips for point-of-care analysis, either in situ or ex situ, in transdermal bodily fluids, namely peripheral blood and interstitial fluid. The ambition is to empower patients, and more generally citizens at any level and place, in health care using high-accuracy self-monitoring systems featuring minimally invasive operation, reduced risk of infection and contamination, and negligible costs.

The potential of microneedle-based biochips is enormous and it can be envisaged that the effort on such a research topic will increase in the next few years, driven by both clinical and market requests for minimally invasive point-of-care systems.

According to the state-of-the-art picture drawn in this review, microneedle-based biochips for transdermal glucose monitoring are now undergoing in vivo trials on humans and it is foreseen that they will be ready for the market in a few years. Biomarker detection with microneedle-based biochips are currently undergoing in vivo validation on animals, and it is likely that in vivo experiments on humans will be carried out in the next years. A few other analytes (both in single and multiplexed configurations) of clinical interest have also been successfully sensed using microneedle-based biochips, but only in vitro operation has been demonstrated in most of the reported cases, thus foreseeing great potential for scientists in the next years in terms of both addressing further analytes and ex vivo/in vivo validation.

As a final consideration, it is our personal opinion that, although still far from practical implementation, integration

Adv. Healthcare Mater. **2015**,
DOI: 10.1002/adhm.201500450

of both drug delivery and sensing capabilities on the same microneedle chip represents the natural outcome in the long-term (next 5–8 years), and a miniaturized artificial pancreas would probably represent the first example of such a technology.

Acknowledgements

The authors acknowledge Dr. Daniela Giannessi at the Institute of Clinical Physiology of the National Research Council (Italy) and Prof. Giovanni Federico at the Department of Clinical and Experimental Medicine of the University of Pisa for fruitful and fertile discussions.

Received: June 15, 2015
Published online:

[1] E. Ichiishi, *Expert Rev. Mol. Diagn.* **2013**, *13*, 331.
[2] E. Menegatti, D. Berardi, M. Messina, I. Ferrante, O. Giachino, B. Spagnolo, G. Restagno, L. Cognolato, D. Roccatello, *Autoimmun. Rev.* **2013**, *12*, 814.
[3] K. K. Jain, *Textbook of Personalized Medicine*, Springer, New York **2015**.
[4] C. Dixit, *J. Biochips Tissue Chips* **2013**, *3*, e124.
[5] World Health Organization, *World Health Statistics 2014*, World Health Organization, Geneva **2014**.
[6] M. Novak, C. Kotanen, S. Carrara, A. Guiseppi-Elie, F. Moussy, *Health Technol.* **2013**, *3*, 271.
[7] S. Kaushik, A. H. Hord, D. D. Denson, D. V. McAllister, S. Smitra, M. G. Allen, M. R. Prausnitz, *Anesth. Analg.* **2001**, *92*, 502.
[8] A. El-Laboudi, N. S. Oliver, A. Cass, D. Johnston, *Diabetes Technol. Ther.* **2013**, *15*, 101.
[9] M. S. Gerstel, V. A. Place, *US3964482 A*, **1976**.
[10] M. Madou, *Fundamentals of Microfabrication: The Science of Miniaturization*, Vol. *1*, CRC Press, USA **2002**.
[11] D. V. McAllister, P. M. Wang, S. P. Davis, J.-H. Park, P. J. Canatella, M. G. Allen, M. R. Prausnitz, *Proc. Natl. Acad. Sci. USA* **2003**, *100*, 13755.
[12] P. Van Damme, F. Oosterhuis-Kafeja, M. Van der Wielen, Y. Almagor, O. Sharon, Y. Levin, *Vaccine* **2009**, *27*, 454.
[13] G. Li, A. Badkar, S. Nema, C. S. Kolli, A. K. Banga, *Int. J. Pharm.* **2009**, *368*, 109.
[14] Y.-C. Kim, J.-H. Park, M. R. Prausnitz, *Adv. Drug Delivery Rev.* **2012**, *64*, 1547.
[15] P. Khanna, J. A. Strom, J. I. Malone, S. Bhansali, *J. Diabetes Sci. Technol.* **2008**, *2*, 1122.
[16] L. Gervais, N. De Rooij, E. Delamarche, *Adv. Mater.* **2011**, *23*, H151.
[17] B. Barry, A. Williams, *Encyclopedia of Pharmaceutical Technology*, Marcel Dekker, New York **1995**, *11*, 449.
[18] F. M. Watt, H. Fujiwara, *Cold Spring Harbor Perspect. Biol.* **2011**, *3*, a005124.
[19] S. M. Jackson, M. L. Williams, K. R. Feingold, P. M. Elias, *West. J. Med.* **1993**, *158*, 279.
[20] C. Harding, A. Watkinson, A. Rawlings, I. Scott, *Int. J. Cosmet. Sci.* **2000**, *22*, 21.
[21] D. J. Tobin, *Chem. Soc. Rev.* **2006**, *35*, 52.
[22] I. M. Braverman, *Microcirculation* **1997**, *4*, 329.
[23] G. Cevc, U. Vierl, *J. Controlled Release* **2007**, *118*, 18.
[24] I. Kupke, B. Kather, S. Zeugner, *Clin. Chim. Acta* **1981**, *112*, 177.
[25] J. N. Roe, B. R. Smoller, *Crit. Rev. Ther. Drug Carrier Syst.* **1998**, *15*, 199.
[26] K. Aukland, R. Reed, *Physiological reviews* **1993**, *73*, 1.
[27] N. Fogh-Andersen, B. M. Altura, B. T. Altura, O. Siggaard-Andersen, *Clinical chemistry* **1995**, *41*, 1522.
[28] T. Koschinsky, K. Jungheim, L. Heinemann, *Diabetes Technol. Ther.* **2003**, *5*, 829.
[29] E. Cengiz, W. V. Tamborlane, *Diabetes Technol. Ther.* **2009**, *11*, S.
[30] Y. Yuan, R. Verma, *Colloids Surf., B* **2006**, *48*, 6.
[31] M. A. Kendall, Y.-F. Chong, A. Cock, *Biomaterials* **2007**, *28*, 4968.
[32] G. W. Dombi, R. C. Haut, W. G. Sullivan, *J. Surg. Res.* **1993**, *54*, 21.
[33] M. L. Crichton, A. Ansaldo, X. Chen, T. W. Prow, G. J. Fernando, M. A. Kendall, *Biomaterials* **2010**, *31*, 4562.
[34] C. Pailler-Mattei, S. Pavan, R. Vargiolu, F. Pirot, F. Falson, H. Zahouani, *Wear* **2007**, *263*, 1038.
[35] M. L. Crichton, X. Chen, H. Huang, M. A. Kendall, *Biomaterials* **2013**, *34*, 2087.
[36] C. Pailler-Mattei, S. Bec, H. Zahouani, *Med. Eng. Phys.* **2008**, *30*, 599.
[37] B. Chua, S. P. Desai, M. J. Tierney, J. A. Tamada, A. N. Jina, *Sens. Actuators, A* **2013**, *203*, 373.
[38] W. Martanto, J. S. Moore, O. Kashlan, R. Kamath, P. M. Wang, J. M. O'Neal, M. R. Prausnitz, *Pharm. Res.* **2006**, *23*, 104.
[39] P. M. Wang, M. R. Prausnitz, W. Martanto, *US20080269666 A1*, **2006**.
[40] H. Vogel, *Biochim. Biophys. Acta, Gen. Subj.* **1972**, *286*, 79.
[41] S. Martin, B. Schneider, L. Heinemann, V. Lodwig, H.-J. Kurth, H. Kolb, W. Scherbaum, *Diabetologia* **2006**, *49*, 271.
[42] A. Shlomowitz, M. D. Feher, *Br. J. Diabetes Vasc. Dis.* **2014**, *14*, 60.
[43] American Diabetes Association, *Diabetes Care* **2010**, *33*, S62.
[44] R. R. Holman, S. K. Paul, M. A. Bethel, D. R. Matthews, H. A. W. Neil, *N. Engl. J. Med.* **2008**, *359*, 1577.
[45] D. C. a. C. T. R. Group, *N. Engl. J. Med.* **2005**, *353*, 2643.
[46] J. L. Kitzmiller, J. M. Block, F. M. Brown, P. M. Catalano, D. L. Conway, D. R. Coustan, E. P. Gunderson, W. H. Herman, L. D. Hoffman, M. Inturrisi, L. B. Jovanovic, S. I. Kjos, R. H. Knopp, M. N. Montoro, E. S. Ogata, P. Paramsothy, D. M. Reader, B. M. Rosenn, A. M. Thomas, M. S. Kirkman, *Diabetes Care* **2008**, *31*, 1060.
[47] K. Kobayashi, H. Suzuki, *Sens. Actuators, B* **2001**, *80*, 1.
[48] Y. Hirokawa, T. Tanaka, *The Journal of chemical physics* **1984**, *81*, 6379.
[49] H. Suzuki, T. Tokuda, K. Kobayashi, *Sens. Actuators, B* **2002**, *83*, 53.
[50] H. Suzuki, T. Tokuda, T. Miyagishi, H. Yoshida, N. Honda, *Sens. Actuators, B* **2004**, *97*, 90.
[51] S. Hirotsu, Y. Hirokawa, T. Tanaka, *J. Chem. Phys.* **1987**, *87*, 1392.
[52] K. Kratz, T. Hellweg, W. Eimer, *Colloids Surf., A* **2000**, *170*, 137.
[53] K. Tsuchiya, N. Nakanishi, E. Nakamachi, in *Proceedings of SPIE, Biomedical Applications of Micro- and Nanoengineering II* (Ed: Dan V. Nicolau), SPIE, Bellingham, WA, **2005**, *5651*, 379.
[54] K. Tsuchiya, N. Nakanishi, Y. Uetsuji, E. Nakamachi, *Biomed. Microdevices* **2005**, *7*, 347.
[55] G. E. Gattiker, K. V. Kaler, M. P. Mintchev, *Microsys. Technol.* **2005**, *12*, 44.
[56] C. G. Li, K. Lee, C. Y. Lee, M. Dangol, H. Jung, *Adv. Mater.* **2012**, *24*, 4583.
[57] K. Lee, H. C. Lee, D.-S. Lee, H. Jung, *Adv. Mater.* **2010**, *22*, 483.
[58] K. Lee, H. Jung, *Biomaterials* **2012**, *33*, 7309.
[59] C. G. Li, C. Y. Lee, K. Lee, H. Jung, *Biomed. Microdevices* **2013**, *15*, 17.
[60] M. Y. Yousif, D. W. Holdsworth, T. L. Poepping, *Exp. Fluids* **2011**, *50*, 769.
[61] Y. Haga, M. Esashi, *Proc. IEEE* **2004**, *92*, 98.
[62] J. R. Windmiller, G. Valdés-Ramírez, N. Zhou, M. Zhou, P. R. Miller, C. Jin, S. M. Brozik, R. Polsky, E. Katz, R. Narayan, J. Wang, *Electroanalysis* **2011**, *23*, 2302.
[63] R. Leuchtner, D. Chrisey, J. Horwitz, K. Grabowski, *Surf. Coat. Technol.* **1992**, *51*, 476.
[64] K. McAteer, R. D. O'Neill, *Analyst* **1996**, *121*, 773.

[65] M. A. Invernale, B. C. Tang, R. L. York, L. Le, D. Y. Hou, D. G. Anderson, *Adv. Healthcare Mater.* **2014**, *3*, 338.
[66] A. Heller, B. Feldman, *Chem. Rev.* **2008**, *108*, 2482.
[67] Y. Yoon, G. S. Lee, K. Yoo, J.-B. Lee, *Sensors* **2013**, *13*, 16672.
[68] J.-H. Kim, K. H. Lee, L. J. Overzet, G. S. Lee, *Nano Lett.* **2011**, *11*, 2611.
[69] S. Zimmermann, D. Fienbork, B. Stoeber, A. W. Flounders, D. Liepmannin, *TRANSDUCERS 2003, 12th International Conference on Solid-State Sensors, Actuators and Microsystems* **2003**, *1*, 99
[70] B. Stoeber, D. Liepmann, *US6406638 B1*, **2002**.
[71] E. Mukerjee, S. Collins, R. Isseroff, R. Smith, *Sens. Actuators, A* **2004**, *114*, 267.
[72] P. M. Wang, M. Cornwell, M. R. Prausnitz, *Diabetes Technol. Ther.* **2005**, *7*, 131.
[73] K. T. Brown, D. G. Flaming, *Advanced Micropipette Techniques for Cell Physiology*, Wiley, Chichester, UK, **1986**.
[74] W. L. Clarke, D. Cox, L. A. Gonder-Frederick, W. Carter, S. L. Pohl, *Diabetes Care* **1987**, *10*, 622.
[75] T. Sato, S. Okada, K. Hagino, Y. Asakura, Y. Kikkawa, J. Kojima, T. Watanabe, Y. Maekawa, K. Isobe, R. Koike, H. Nakajima, K. Asano, *Diabetes Technol. Ther.* **2011**, *13*, 1194.
[76] K. Sakaguchi, Y. Hirota, N. Hashimoto, W. Ogawa, T. Sato, S. Okada, K. Hagino, Y. Asakura, Y. Kikkawa, J. Kojima, Y. Maekawa, H. Nakajima, *Diabetes Technol. Ther.* **2012**, *14*, 485.
[77] K. Sakamoto, F. Kubo, K. Yoshiuchi, A. Ono, T. Sato, K. Tomita, K. Sakaguchi, M. Matsuhisa, H. Kaneto, H. Maegawa, H. Nakajima, A. Kashiwagi, K. Kosugi, *J. Diabetes Invest.* **2013**, *4*, 552.
[78] R. O. Potts, M. J. Tierney, *EP1309271 A1*, **2003**.
[79] M. Hunter, A. Enejder, T. Scecina, M. Feld, W. C. Shih, *US20070060806 A1*, **2007**.
[80] S. S. Mitragotri, J. Kost, S. C. Kellogg, N. F. Warner, T. A. Elstrom, *US20130035566 A1*, **2013**.
[81] P. Khanna, K. Luongo, J. A. Strom, S. Bhansali, *J. Micromech. Microeng.* **2010**, *20*, 045011.
[82] A. Jina, B. L. Chua, S. Desai, A. Parmar, A. N. Kawde, *US20080058726 A1*, **2008**.
[83] A. N. Jina, *US8280476 B2*, **2012**.
[84] O. A. Shergold, N. A. Fleck, *Proc. R. Soc. London, Ser. A* **2004**, *460*, 3037.
[85] A. N. Jina, M. J. Tierney, J. A. Tamada, S. McGill, S. Desai, B. Chua, A. Chang, M. Christiansen, *J. Diabetes Sci. Technol.* **2014**, *8*, 483.
[86] G. Valdés-Ramírez, Y.-C. Li, J. Kim, W. Jia, A. J. Bandodkar, R. Nuñez-Flores, P. R. Miller, S.-Y. Wu, R. Narayan, J. R. Windmiller, R. Polsky, J. Wang, *Electrochem. Commun.* **2014**, *47*, 58.
[87] R. Bullen, T. Arnot, J. Lakeman, F. Walsh, *Biosens. Bioelectron.* **2006**, *21*, 2015.
[88] E. Katz, *Implantable Bioelectronics*, John Wiley & Sons, Hoboken, NJ **2014**.
[89] M. Zhou, J. Wang, *Electroanalysis* **2012**, *24*, 197.
[90] J. R. Windmiller, N. Zhou, M.-C. Chuang, G. Valdés-Ramírez, P. Santhosh, P. R. Miller, R. Narayan, J. Wang, *Analyst* **2011**, *136*, 1846.
[91] L. Strambini, A. Longo, S. Scarano, T. Prescimone, I. Palchetti, M. Minunni, D. Giannessi, G. Barillaro, *Biosens. Bioelectron.* **2015**, *66*, 162.
[92] L. M. Strambini, A. Longo, A. Diligenti, G. Barillaro, *Lab Chip* **2012**, *12*, 3370.
[93] International Organization for Standardization, *In vitro Diagnostic Test Systems: Requirements for Blood-glucose Monitoring Systems for Self-Testing in Managing Diabetes Mellitus*, ISO, Geneva, CH, **2003**.
[94] R. Etzioni, N. Urban, S. Ramsey, M. McIntosh, S. Schwartz, B. Reid, J. Radich, G. Anderson, L. Hartwell, *Nat. Rev. Cancer* **2003**, *3*, 243.
[95] P. Yager, G. J. Domingo, J. Gerdes, *Annu. Rev. Biomed. Eng.* **2008**, *10*, 107.
[96] A. Taddio, M. Ipp, S. Thivakaran, A. Jamal, C. Parikh, S. Smart, J. Sovran, D. Stephens, J. Katz, *Vaccine* **2012**, *30*, 4807.
[97] S. R. Corrie, G. J. Fernando, M. L. Crichton, M. E. Brunck, C. D. Anderson, M. A. Kendall, *Lab Chip* **2010**, *10*, 2655.
[98] K. Sauermann, S. Jaspers, U. Koop, H. Wenck, *BMC Dermatol.* **2004**, *4*, 13.
[99] D. A. Muller, S. R. Corrie, J. Coffey, P. R. Young, M. A. Kendall, *Anal. Chem.* **2012**, *84*, 3262.
[100] A. C. Schmidt, *N. Engl. J. Med.* **2010**, *363*, 484.
[101] M. Flamand, F. Megret, M. Mathieu, J. Lepault, F. A. Rey, V. Deubel, *J. Virol.* **1999**, *73*, 6104.
[102] P. R. Young, P. A. Hilditch, C. Bletchly, W. Halloran, *J. Clin. Microbiol.* **2000**, *38*, 1053.
[103] A. Bhargav, D. A. Muller, M. A. Kendall, S. R. Corrie, *ACS Appl. Mater. Interfaces* **2012**, *4*, 2483.
[104] J. W. Coffey, S. R. Corrie, M. A. Kendall, *Biomaterials* **2013**, *34*, 9572.
[105] J.-H. Park, M. G. Allen, M. R. Prausnitz, *J. Controlled Release* **2005**, *104*, 51.
[106] B. Yeow, J. W. Coffey, D. A. Muller, L. Grøndahl, M. A. Kendall, S. R. Corrie, *Anal. Chem.* **2013**, *85*, 10196.
[107] D. Jenkins, S. Corrie, C. Flaim, M. Kendall, *RSC Adv.* **2012**, *2*, 3490.
[108] A. V. Romanyuk, V. N. Zvezdin, P. Samant, M. I. Grenader, M. Zemlyanova, M. R. Prausnitz, *Anal. Chem.* **2014**, *86*, 10520.
[109] A. Skeel, T. Yoshimura, S. D. Showalter, S. Tanaka, E. Appella, E. Leonard, *J. Exp. Med.* **1991**, *173*, 1227.
[110] K. N. Olsen, B. B. Budde, H. Siegumfeldt, K. B. Rechinger, M. Jakobsen, H. Ingmer, *Appl. Environ. Microbiol.* **2002**, *68*, 4145.
[111] O. Siggaard-Andersen, *Encyclopedia of Respiratory Medicine* 2006, Elsevier-Academic Press, New York, **2006**, 5.
[112] B. S. Meldrum, *J. Nutr.* **2000**, *130*, 1007S.
[113] B. Ahlborg, J. Bergstrom, L.-G. Ekelund, E. Hultman, *Acta Physiol. Scand.* **1967**, *70*, 129.
[114] D. F. Bohr, *Pharmacol. Rev.* **1964**, *16*, 85.
[115] I. Park, Z. Li, X. Li, A. P. Pisano, R. S. Williams, *Biosens. Bioelectron.* **2007**, *22*, 2065.
[116] F. B. Loiselle, J. R. Casey, in *Membrane Transporters in Drug Discovery and Development*, Vol. *637* (Ed: Q. Yan), Humana Press, New York City **2010**, p. 311.
[117] P. Capuano, G. Capasso, *G. Ital. Nefrol.* **2002**, *20*, 139.
[118] A. Kotyk, J. Slavik, *Intracellular pH and its Measurement*, CRC Press, Boca Raton, FL **1989**.
[119] Y. Cui, Q. Wei, H. Park, C. M. Lieber, *Science* **2001**, *293*, 1289.
[120] G. Zheng, F. Patolsky, Y. Cui, W. U. Wang, C. M. Lieber, *Nat. Biotechnol.* **2005**, *23*, 1294.
[121] I. Svancara, K. Vytras, K. Kalcher, A. Walcarius, J. Wang, *Electroanalysis* **2009**, *21*, 7.
[122] M. I. Lindinger, J. M. Kowalchuk, G. J. Heigenhauser, *Am. J. Physiol.: Regul., Integr. Comp. Physiol.* **2005**, *289*, R891.
[123] EnvisionTEC e-Shell 200 Series, http://envisiontec.com/3d-printing-materials/perfactory-materials/e-shell-200-series/(accessed: June 2015).
[124] S. D. Gittard, A. Ovsianikov, N. A. Monteiro-Riviere, J. Lusk, P. Morel, P. Minghetti, C. Lenardi, B. N. Chichkov, R. J. Narayan, *J. Diabetes Sci. Technol.* **2009**, *3*, 304.
[125] G. Nagesh Babu, M. Bawari, V. Mathur, J. Kalita, U. Misra, *Clin. Chim. Acta* **1998**, *273*, 195.
[126] E. Valencia, A. Marin, G. Hardy, *Nutrition* **2002**, *18*, 367.
[127] R. Esfandyarpour, H. Esfandyarpour, M. Javanmard, J. S. Harris, R. W. Davis, *Sens. Actuators, B* **2013**, *177*, 848.

[128] P. R. Miller, X. Xiao, I. Brener, D. B. Burckel, R. Narayan, R. Polsky, *Adv. Healthcare Mater.* **2014**, *3*, 876.
[129] B. M. Koeppen, B. A. Stanton, *Renal Physiology: Mosby Physiology Monograph Series*, Elsevier Health Sciences, Philadelphia, PA **2012**.
[130] P. Vazquez, G. Herzog, C. O'Mahony, J. O'Brien, J. Scully, A. Blake, C. O'Mathúna, P. Galvin, *Sens. Actuators, B* **2014**, *201*, 572.
[131] D. W. Arrigan, *Anal. Lett.* **2008**, *41*, 3233.
[132] G. Herzog, V. Beni, *Anal. Chim. Acta* **2013**, *769*, 10.
[133] J. G. Baker, S. J. Hill, R. J. Summers, *Trends Pharmacol. Sci.* **2011**, *32*, 227.
[134] D. Coltart, D. Shand, *Br. Med. J.* **1970**, *3*, 731.
[135] P. R. Miller, S. D. Gittard, T. L. Edwards, D. M. Lopez, X. Xiao, D. R. Wheeler, N. A. Monteiro-Riviere, S. M. Brozik, R. Polsky, R. J. Narayan, *Biomicrofluidics* **2011**, *5*, 013415.
[136] C. B. Jacobs, M. J. Peairs, B. J. Venton, *Anal. Chim. Acta* **2010**, *662*, 105.
[137] A. Grano, M. C. De Tullio, *Med. Hypotheses* **2007**, *69*, 953.
[138] S. D. Gittard, R. Narayan, J. Lusk, P. Morel, F. Stockmans, M. Ramsey, C. Laverde, J. Phillips, N. A. Monteiro-Riviere, A. Ovsianikov, B. N. Chichkov, *Biotechnol. J.* **2009**, *4*, 129.
[139] J.-W. Choi, R. Wicker, S.-H. Lee, K.-H. Choi, C.-S. Ha, I. Chung, *J. Mater. Process. Technol.* **2009**, *209*, 5494.
[140] D. Wolter, *Aktuelle Probl. Chir.Orthop.* **1982**, *26*, 28.
[141] R. Bader, E. Steinhauser, H. Rechl, W. Siebels, W. Mittelmeier, R. Gradinger, *Orthopade* **2003**, *32*, 32.
[142] P. R. Miller, S. A. Skoog, T. L. Edwards, D. M. Lopez, D. R. Wheeler, D. C. Arango, X. Xiao, S. M. Brozik, J. Wang, R. Polsky, R. J. Narayan, *Talanta* **2012**, *88*, 739.
[143] P. R. Miller, S. A. Skoog, T. L. Edwards, D. R. Wheeler, X. Xiao, S. M. Brozik, R. Polsky, R. J. Narayan, *J. Visualized Exp.* **2012**, *64*, e4067.
[144] A. N. Jina, *WO2006105146 A2*, **2006**.
[145] S. Y. Yang, E. D. O'Cearbhaill, G. C. Sisk, K. M. Park, W. K. Cho, M. Villiger, B. E. Bouma, B. Pomahac, J. M. Karp, *Nat. Commun.* **2013**, *4*, 1702.